Oxygen isotope systematics of the Banda Arc: Low delta O-18 despite involvement of subducted continental material in magma genesis.

Vroon, P.Z.; Lowry, D.; van Bergen, M.J.; Boyce, A.J.; Mattey, D.P.

published in
Geochimica et Cosmochimica Acta
2001

DOI (link to publisher)
10.1016/S0016-7037(00)00554-8

document version
Publisher's PDF, also known as Version of record

Pergamon

Geochimica et Cosmochimica Acta, Vol. 65, No. 4, pp. 589–609, 2001

0016-7037/01 $20.00 + .00

PII S0016-7037(00)00554-8

Oxygen isotope systematics of the Banda Arc: Low $\delta^{18}O$ despite involvement of subducted continental material in magma genesis

P. Z. VROON,[1,*,†] D. LOWRY,[1] M. J. VAN BERGEN,[2] A. J. BOYCE,[3] and D. P. MATTEY[1]

[1]Department of Geology, Royal Holloway University of London, Egham Hill, Egham, Surrey TW20 0EX, United Kingdom
[2]Faculty of Earth Sciences, University of Utrecht, P.O. Box 80.021, 3508 TA Utrecht, The Netherlands
[3]Scottish Universities Environmental Research Centre, Scottish Enterprise Technology Park, East Kilbride, Glasgow, G75 0QF, Scotland

(*Received January* 26, 2000; *accepted in revised form September* 18, 2000)

Abstract—This study reports new laser fluorination oxygen isotope data for 60 volcanic rocks and 15 sediments distributed over the whole length of the Banda Arc, eastern Indonesia. The melt oxygen isotope values ($\delta^{18}O_{melt}$) were calculated from phenocryst $\delta^{18}O$ data using theoretical and empirical mineral-melt fractionation factors. The $\delta^{18}O_{melt}$ of individual volcanic centers within the arc varies between 5.57 and 6.54‰, except for Serua ($\delta^{18}O_{melt}$ = 6.13–7.48‰) and Ambon ($\delta^{18}O_{melt}$ = 8.12–8.38‰). These $\delta^{18}O_{melt}$ values are up to 2‰ lower than new and previously published oxygen isotope data obtained on whole-rock powders by conventional methods. We attribute this discrepancy to post-emplacement low-temperature alteration and/or to a systematic deviation of the bulk analysis. Sediment $\delta^{18}O_{wr}$ (calculated from the $\delta^{18}O$ carbonate and silica fractions, both measured conventionally) range between 12.9 and 24.2‰. The low $\delta^{18}O_{melt}$ values (excluding Serua and Ambon) overlap with the mantle range, and are in agreement with simple two-component source-mixing models that predict 1–5% addition of subducted continental material to a depleted MORB-type source in the sub-arc mantle. This percentage is consistent with previous models based on Sr–Nd–Pb–Th–He–Hf isotope data. However, correlations between incompatible trace-element ratios and oxygen isotope systematics requires involvement of partial melts derived from subducted continental material as the major slab component rather than bulk addition. The contribution of hydrous fluids, from both subducted altered oceanic crust and continental material is probably of minor importance. Magma-mantle wedge interaction models could account for the observed low $\delta^{18}O$ signatures, but predicted effects are difficult to distinguish from models without mantle-wedge interaction. Assimilation of arc-crust material is thought to be important for the high $\delta^{18}O_{melt}$ values of Serua and Ambon. AFC modelling suggests up to 20% and 80% assimilation at Serua and Ambon, respectively. Inclusions of meta-sedimentary material and whole-rock Sr–Nd isotopes point to assimilation processes at Nila, but this probably had little effect on the $\delta^{18}O$ of phenocrysts, which record original source values. According to radiogenic isotope data, magma sources in the Banda Arc are the most heavily influenced by fluxes of subducted continental material among currently active oceanic island arcs. Hence, the results of this study suggest that high $\delta^{18}O$ (>6.5‰) in arc lavas are difficult to reconcile with addition of subducted components to magma sources, but must reflect assimilation of arc crustal material.

1. INTRODUCTION

One of the salient features of magmatism at converging plate boundaries is the large diversity in geochemical signatures that can be observed on different spatial scales, ranging from individual volcanic centers to entire arc systems. First-order variations can be attributed to physical and chemical parameters that are specific for a particular subduction setting and exert controls on the involvement of magma-source components, the slab-to-wedge transfer mode of subducted components, melt-extraction processes and subsequent modifications en-route to the surface. This large number of factors precludes a uniform model for arc magma genesis, and calls for a case-by-case approach in distinct arc settings.

Among the parameters that determine the trace-element chemistry of island-arc magmas, the transfer mechanism from slab to wedge (fluid versus melt, Ellam et al., 1988; Hoogewerff et al., 1997; Elliott et al., 1997) and the composition and quantity of subducted sediments (Plank and Langmuir, 1993) appear to be of prime importance. Variations in input from subducted material create a spectrum of island arcs between two end-members: settings with little or no supply of sediments and settings where sediment subduction is dominant. The Banda Arc is an extreme example of the latter group, as it represents an arc system where sediment supply is strongly enhanced by the approach of a passive continental margin. Large contributions from subducted continental material (terrigenous sediments and/or continental crust) to magma sources have been revealed by trace-element and isotopic studies (Whitford et al., 1977; 1981; Whitford and Jezek, 1979; Gill and Williams, 1990; Hilton et al., 1989; 1992; Vroon, 1992; Vroon et al., 1993; 1995; 1998), whereas the influence of subducted (altered) oceanic crust is thought to be of minor importance.

Generally, the budget of subducted continental material (SCM) involvement inhibits the analysis of the mode of slab-to-wedge transfer solely from incompatible trace-element signatures, because any slab-derived signal dominates the final source-mixing product, given the large contrasts in element

* Author to whom correspondence should be addressed.
† *Present address:* Faculteit Aardwetenschappen, Vrije Universiteit, De Boelelaan 1085, 1081 HV Amsterdam, The Netherlands (vrop@geo.vu.nl).

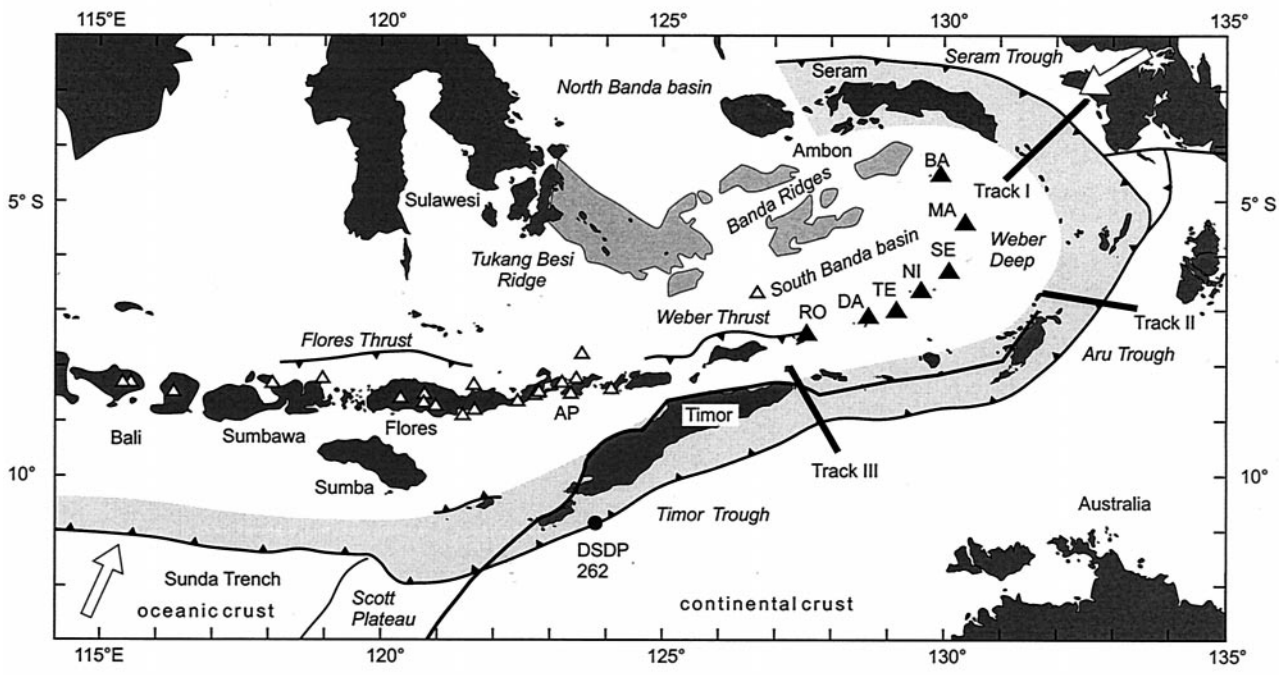

Fig. 1. Map of Eastern Indonesia after Hamilton (1979) and Honthaas et al. (1998), showing the Banda Arc volcanoes as solid triangles and other active volcanoes as open triangles. Arrows indicate plate movements relative to the Southeast Asian plate (DeMets et al., 1994; Tregoning et al., 1994; Puntodewo et al., 1994). Tracks I, II, III, and DSDP 262 are sediment sample locations (see Vroon, 1992 and Vroon et al., 1995). Abbreviations: BA = Banda Archipelago, MA = Manuk, SE = Serua, NI = Nila, TE = Teon, DA = Damar, RO = inactive Romang, AP = Adonara–Pantar segment. Shaded areas indicate the accretionary wedge and the submerged Banda Ridges.

abundances with (depleted) mantle wedge material. In this respect, oxygen may be a more suitable tracer, because of its compatible behavior and limited concentration contrast. Furthermore, the potential of oxygen as an indicator of recycled subducted material is supported by the slight enrichment in ^{18}O of oceanic island-arc basalts (average $\delta^{18}O = 6.0 \pm 0.3$), compared to MORB ($5.7 \pm 0.2$) and OIB ($5.5 \pm 0.5$), based on conventional oxygen isotope data (Harmon and Hoefs, 1995). We therefore explore oxygen-isotope signals, in combination with Sr–Nd isotopes and trace-element ratios, to infer source-contamination processes in the Banda Arc.

A previous oxygen isotope study of the Banda Arc, using conventional analytical techniques, revealed the existence of considerable variations in $\delta^{18}O$ and $^{87}Sr/^{86}Sr$ signatures, which were interpreted in terms of contributions of subducted continent-derived sediments to magma sources (Magaritz et al., 1978). These results provided a starting point for a detailed study of oxygen isotope systematics by the laser-fluorination (LF) technique, which has the advantage of producing high yields (>98%), and is thus likely to give more accurate results (Mattey and Macpherson, 1993). Furthermore, the LF technique uses separates of phenocrysts, which are less sensitive to low-temperature alteration and secondary water up-take than bulk rocks. The new LF data reported here cover all active volcanoes and two extinct volcanic islands (Ambon and Romang) in the Banda Arc, allowing an arc-wide evaluation of magmatic oxygen isotope signatures. Within-suite trends establish the extent to which arc-crust assimilation plays a role in individual centers. The results will be discussed, in combination with Sr–Nd–Pb isotope and trace-element data obtained on the same volcanic and sediment samples (Vroon, 1992; Vroon et al., 1993; Vroon et al., 1995), to distinguish mechanisms by which subducted continental material is transferred to magma sources in the sub-arc mantle.

2. TECTONIC BACKGROUND OF THE BANDA ARC

The Banda Arc is the eastward continuation of the Sunda Arc. Two plates are subducting beneath the Banda Arc (Fig. 1). In the south, the Indian–Australian plate enters the subduction zone at a velocity of 6–7 cm/y in a NNE direction (DeMets et al., 1994; Tregoning et al., 1994), whereas in the north, parts of the continental crust of Irian Jaya enter the Seram trench in a WSW direction (relative to the Australian plate) at a velocity of 9–10 cm/y (Puntodewo et al., 1994). In contrast to the Sunda Arc, where Indian oceanic crust enters the subduction zone, the Banda Arc trenches are underlain by Australian continental crust. How far this continental crust has entered the subduction zone is still a matter of debate (cf. Van Bergen et al., 1993). Most likely the leading edge of the continental margin has penetrated deepest into the system near Timor, near the arc sector where volcanic activity ceased some 3 million years ago (Abbott et al., 1981; Honthaas et al., 1998).

The Banda Sea region is composed of two basins (water-depth >5000 m): the South Banda Basin and the North Banda Basin, which are separated by the Banda ridges. Different origins have been postulated for the Banda Sea basins: (1) trapped Jurassic–Cretaceous fragments of Indian Ocean crust

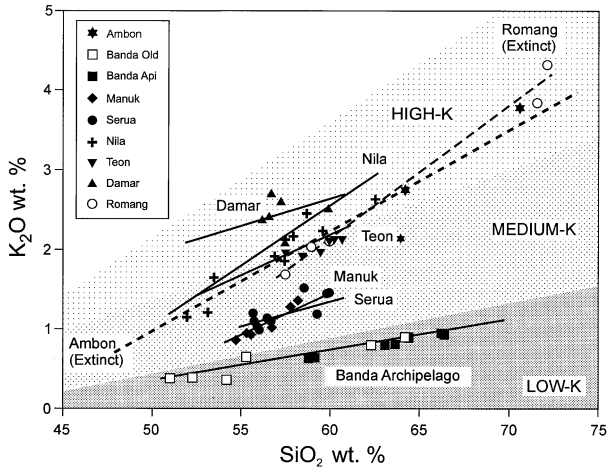

Fig. 2. SiO_2 versus K_2O diagram for Banda Arc volcanic rocks. Classification after Gill (1981). Note the increase of K_2O from NE to SW along the arc and the steep trends for Ambon, Nila, and Romang. Symbols indicate samples used in this study, whereas regression lines represent all samples studied by Vroon (1992). The Ambon regression line is based on unpublished data (Utrecht).

(e.g., Bowin et al., 1980; Pigram and Panggabean, 1983; Lapouille et al., 1985); (2) the South Banda Basin as part of the Indian Oceanic crust and the North Banda Basin as remnant of the Molluca Sea plate (e.g., Silver et al., 1985); and (3) a back-arc spreading origin (e.g., Hamilton, 1979; Honthaas et al., 1998). Refraction studies (Jacobson et al., 1978) indicate crustal thicknesses up to 15 km. Thicknesses of the sediment cover are highly variable. Hamilton (1979) observed layered sediments in seismic refraction studies, presumably turbidites and volcaniclastic aprons, which fill the local topographic low areas. Pelagic sediments mantle the irregular topography, and are about 200 m thick in the western and thinner in the eastern part of the South Banda Basin. Bowin et al. (1980) reported a maximum thickness of the sediment pile of 2 km.

The northeast trending topographic highs in the central Banda Sea basin, the Lucipara or Banda ridges, are composed of continental and volcanic rocks (Silver et al., 1985; Honthaas et al., 1998; Fig. 1). Dredge recoveries included basalts, andesites, meta-sediments, volcaniclastic sediments and metamorphosed rocks, which resemble formations on Irian Jaya (Silver et al., 1985). The volcanic rocks vary in age between 3.5 and 7 Ma (Silver et al., 1985; Honthaas et al., 1998).

The volcanic Banda Arc emerges from a narrow ridge between the Weber Deep in the east and the South Banda Basin in the west. The Banda Archipelago is built on a triangular platform, separated from the rest of the arc by 4000 m waterdepth. The other volcanic islands are located on a narrow ridge. All are strato-volcanoes and the Banda Api and Nila volcanoes include caldera structures.

3. PETROLOGICAL AND GEOCHEMICAL CHARACTERISTICS OF THE BANDA ARC VOLCANIC ROCKS

The Banda Arc rocks can be divided into three groups based on their SiO_2–K_2O variations (Fig. 2; cf. Van Bergen et al., 1989; Vroon et al., 1993): (1) low-K Banda Archipelago, and (2) medium-K Serua and Manuk, both with phenocryst assemblages of olivine, clinopyroxene, orthopyroxene, plagioclase and Fe–Ti oxides, and (3) high-K Nila, Teon and Damar, containing, in addition to these phases, amphibole and biotite. The extinct volcanic islands of Ambon and Romang are intermediate between the two latter groups. Andesites are the most common rock types (SiO_2 = 55–65 wt.%), whereas basalts are scarce. Dacitic and rhyolitic rocks have only been found on the islands of Ambon, Banda Archipelago and Romang. The volcanic rocks from Ambon, Nila and Romang display steep trends in the SiO_2–K_2O diagram crossing the boundaries of normal calc-alkaline fractionation series (Fig. 2). This could be an indication of assimilation.

The Banda Arc is characterized by large variations in Sr–Nd–Pb isotopes (Magaritz and Jezek, 1978; Whitford and Jezek, 1979; Whitford et al., 1981; Vroon et al., 1993). $^{87}Sr/^{86}Sr$ and Pb isotope ratios increase along the arc from NE to SW, whereas the $^{143}Nd/^{144}Nd$ ratios decrease in the same direction (Fig. 3). Both Sr and Nd isotopes display large within-suite variations in Serua, Nila, Teon, and Romang, whereas Pb isotope variations are limited (Vroon et al., 1993).

4. OXYGEN ISOTOPIC DATA

4.1. Analytical Procedures

4.1.1. Volcanic rocks

Rocks were broken to <5 mm diameter with a tungsten carbide-coated jaw crusher. The powder was subsequently sieved for a fraction of 125–250 μm or 250–355 μm. The sieved fraction was ultrasonically cleaned with distilled water and dried. Crystal fragments with oxide inclusions were removed with a Frantz magnet. The remaining groundmass was removed by heavy liquid (ρ = 2.8 g · cm^{-3}) separation. Mineral separates of 1–2 mg were collected by handpicking under a binocular microscope. Only clear crystals, without inclusions, alteration rims, and cracks were selected. In general, 10–20 crystal fragments were used for a single analysis.

The laser-fluorination (LF) technique used in this study was described by Mattey and Macpherson (1993). Minerals (ca. 1.5 ± 0.3 mg) were heated with a Nd–YAG laser in the presence of ClF_3. Oxygen is converted to CO_2 over hot graphite. The results are reported as per mil deviations relative to the SMOW standard. The LF oxygen isotope data are calibrated to NBS-30 biotite = 5.1‰. Accuracy and precision for three oxygen isotope standards are shown in Table 1. Blanks are less than 0.25%; runs with yields less than 95% were rejected. Replicate analyses of standards fall within 0.3‰ (2 s.d.).

Ten whole rock powders were analyzed by the conventional oxygen isotope technique at Utrecht University following the procedure described by Clayton and Mayeda (1963). Details of the silicate oxygen extraction line in Utrecht are given in De Groot (1993). Precision of the results is ±0.3‰ (2 s.d.).

Additional Sr isotopes were measured at RHBNC and Free University, Amsterdam. Approximately 3 mg of clinopyroxene from the same separates as used for the oxygen isotopes were analyzed on a VG354 (RHBNC) or MAT262 (VU-Amsterdam) after standard chemical procedures. Measured values for NIST SRM-987 were 0.710249 ± 21 (2 s.d., n = 65) and

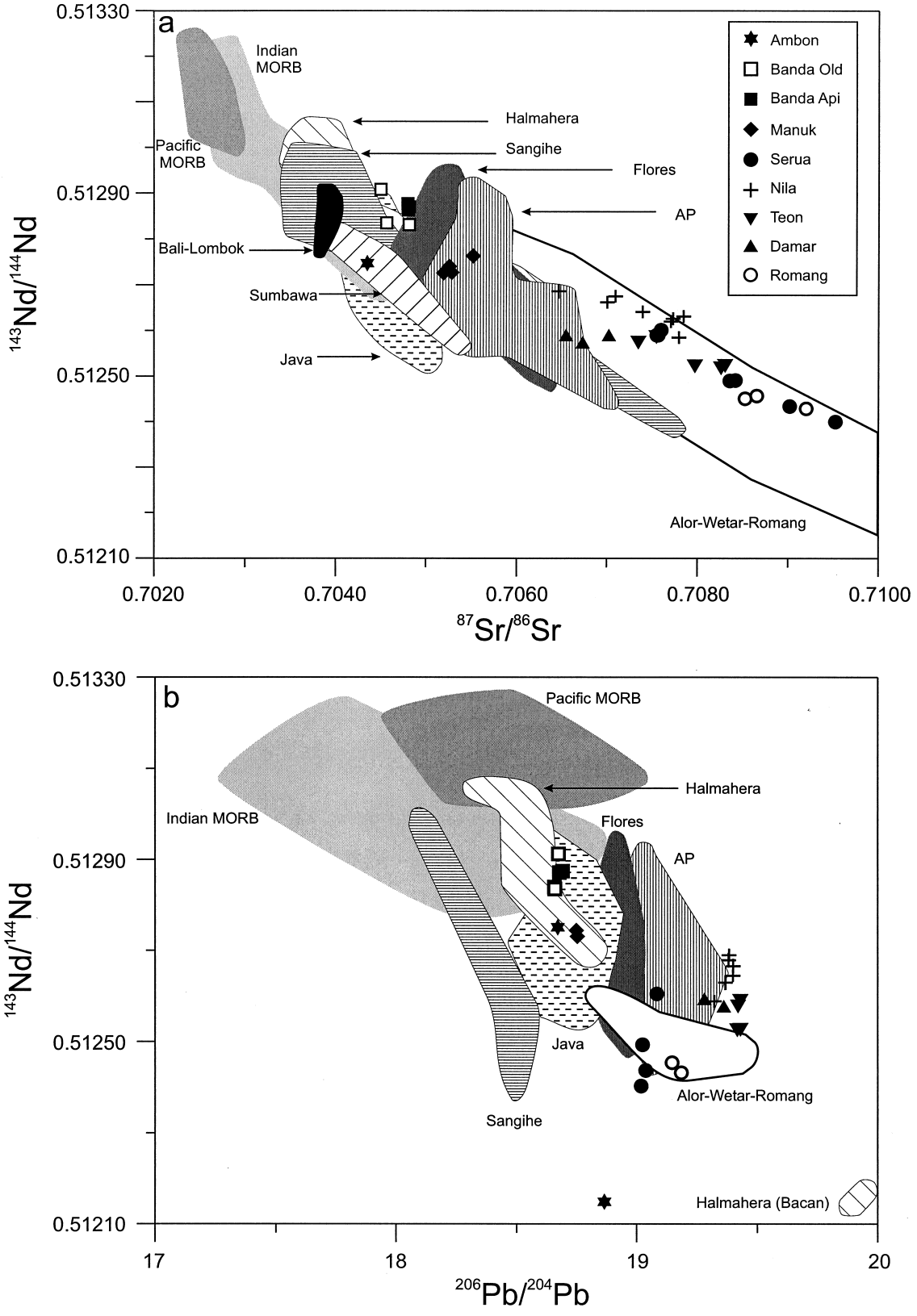

Fig. 3. $^{87}Sr/^{86}Sr$–$^{143}Nd/^{144}Nd$ (a) and $^{206}Pb/^{204}Pb$–$^{143}Nd/^{144}Nd$ (b) diagrams for Banda Arc volcanics (Vroon et al., 1993). Note the large within-suite variations for Serua and Nila. Data sources for the Banda Arc: Vroon et al. (1993), for Java and Flores: Edwards et al. (1991; 1994), Adonara–Pantar (AP): Hoogewerff et al. (1997), and for Ambon, Alor–Wetar and the Sangihe Arc: unpublished data (Utrecht), 1992–1999.

Table 1. Results for oxygen-isotope standards. Reported errors are 2 standard deviations. #The relatively poor yield for NIST NBS-30 is due to the difficulty of keeping all biotite flakes in the sample holder during reaction with the laser (e.g., Mattey and Macpherson, 1993).

Standard	Material	$\delta^{18}O$ (‰) this study	n	Yield (%)	$\delta^{18}O$ (‰) literature	Reference
NIST NBS-30	biotite	5.10 ± 0.10	10	>90#	5.04	Mattey and Macpherson (1993)
UWG-2	garnet	5.81 ± 0.12	7	>99	5.8	Valley et al. (1995)
San Carlos (SC)	olivine	4.86 ± 0.15	119	>99	4.88	Mattey and Macpherson (1993)

0.710245 ± 11 (2 s.d., $n = 13$), respectively. All data reported in Tables 2 and 3 are relative to NIST SRM-987 = 0.710240.

4.1.2. Sedimentary rocks

Fifteen sediment samples were selected for stable isotopic analyses of silicate ($\delta^{18}O$) and carbonate ($\delta^{13}C$ and $\delta^{18}O$) at SUERC (East Kilbride, UK). Each sample was placed in a plasma asher for a minimum of 2 hours (Polaron Plasma Asher E2000). This low enthalpy technique facilitated the removal of organic material. The samples were then dried and analyzed for silicate oxygen using standard procedures (Clayton and Mayeda, 1963; Borthwick and Harmon, 1982). The remaining fraction was analyzed for carbonate $\delta^{13}C$ and $\delta^{18}O$, via whole-rock acid digestion following the method of McCrea (1950), using an overnight reaction at 25°C, as XRD analyses had previously indicated the presence of only calcite. All product CO_2 gases were analyzed on a VG Sira 10 mass spectrometer, and standard correction factors were applied to the raw data (e.g., Craig, 1957). Analytical reproducibility for $\delta^{18}O$ and $\delta^{13}C$ was better than ±0.3‰ (2 s.d.) for these samples. Results are reported as per mil deviations relative to the SMOW and PDP standards.

Additional Sr isotopes were measured on the same silica fraction on which oxygen isotopes were determined, following procedures described above.

4.2. Oxygen Isotopic Composition of the Banda Arc Lavas

4.2.1. Oxygen isotope signatures from laser fluorination data

Samples were selected to cover within-suite variations of the individual volcanoes, based on a large geochemical database (Vroon, 1992; Vroon et al., 1993; 1995). Many samples contain clinopyroxene (47 determinations) and orthopyroxene (37), whereas olivine (16) is less abundant. The hydrous minerals amphibole (4) and biotite (5) only appear in the high-K lavas in the southern part of the arc. Measured oxygen isotope compositions are given in Table 2 and are illustrated in Fig. 4. The $\delta^{18}O$ values of different phenocryst types from individual samples increase in the order olivine–clinopyroxene–orthopyroxene or amphibole–clinopyroxene–orthopyroxene, as can be expected from fractionation systematics under equilibrium conditions. Disequilibrium is observed in a few samples from the Banda Archipelago (BB21A3 and BB28), which show a reversed order of clinopyroxene and olivine, possibly as a result of minor alteration.

There are no clear within-suite trends for a single phenocryst type as a function of bulk-rock SiO_2, due to the limited compositional ranges, which would theoretically correspond to only minor changes in $\delta^{18}O$ if magmas evolved through crystal fractionation, and due to the analytical errors involved. The Banda Archipelago lavas (Banda Old and Banda Api) cover a significant compositional range, but $\delta^{18}O$ values of phenocrysts remain fairly constant. Exceptional $\delta^{18}O$ variations are observed in the samples from Serua, despite the narrow SiO_2 range.

In view of the evolved nature of the Banda Arc lavas, the observed $\delta^{18}O$ signatures will be higher than primary parental magmas, but theoretical fractionation predict that deviations will not exceed about 0.3‰ (see below). In this respect, it is of interest to note that $\delta^{18}O$ values of most of the Banda olivines overlap with those of olivines measured in more primitive island-arc lavas (Eiler et al., 2000).

In order to facilitate comparison with conventional whole-rock data, oxygen isotope compositions of the melts ($\delta^{18}O_{melt}$) have been calculated from $\delta^{18}O$ determined on phenocrysts (Table 2). This conversion from $\delta^{18}O$ mineral to $\delta^{18}O$ melt allows a comparison of oxygen-isotope signatures within the Banda Arc as well as with island arcs for which only whole-rock data have been reported. We have used the coefficients of Kalimarides (1985) and Zheng (1993a; 1993b) to convert olivine (ol), orthopyroxene (opx), clinopyroxene (cpx), amphibole (amph), and biotite (bi) $\delta^{18}O$ values to $\delta^{18}O_{melt}$ values. The calculated values are based on the assumption that (1) all minerals and the melt were in equilibrium; (2) the temperature was about 1300 K; (3) magmas behaved as a closed system.

(1) Most of the Banda Arc lavas have phenocryst assemblages that are in mutual equilibrium for $\delta^{18}O$. Figure 5 shows Δ values of the mineral pairs cpx–opx and cpx–ol as measured in individual samples ($\Delta_{i-j} = \delta^{18}O_i - \delta^{18}O_j$). In the Banda Arc as a whole, the differences are $\Delta_{cpx-ol} = 0.47 \pm 0.27$‰ (1 s.d., $n = 12$), $\Delta_{opx-cpx} = 0.16 \pm 0.12$‰, (1 s.d., $n = 30$). The $\Delta_{opx-cpx}$ values suggest equilibrium at magmatic temperatures, except for Serua, where $\Delta_{opx-cpx}$ tends to be too high. The Δ_{cpx-ol} values for the Banda Archipelago, Manuk, and Serua (sample SE26A) also show equilibrium, but the mineral pair is clearly out of equilibrium in samples SE9A3 (Serua) and NI16 (Nila). In the latter cases we have only converted the $\delta^{18}O_{cpx}$ data, assuming that this yields the most reliable approximation of $\delta^{18}O_{melt}$.

(2) Although magmatic temperatures will vary with fractionation, the temperature effect is negligible on $\Delta_{opx-cpx}$, and <0.1‰ on Δ_{cpx-ol} at $T = 1100$–1500 K (see Fig. 5). Considering the predominantly andesitic rock compositions and the analytical errors involved, we therefore believe that a temperature of ~1300 K is sufficiently representative to calculate the $\delta^{18}O_{melt}$ values from mineral data.

Table 2. Oxygen-isotope results for Banda Arc volcanics relative to SMOW. Additional Sr–Nd–Pb isotope data are from Vroon et al. (1993), except those with reported errors, which were analyzed at RHBNC. All Sr-isotope data are relative to NIST SRM-987 = 0.710240. Analytical details can be found in Vroon et al. (1996). Underlined oxygen-isotope data are from conventional whole-rock (wr) analyses of powders (see analytical procedures). $\delta^{18}O_{melt}$ values are calculated from the $\delta^{18}O_{cpx,opx,hbl,bi,ol}$ values assuming $\Delta_{1-opx} = 0.30$, $\Delta_{1-cpx} = 0.39$, $\Delta_{1-ol} = 0.79$, $\Delta_{1-hbl} = 0.45$, $\Delta_{1-bi} = 0.52$, based on Kalamarides (1986) and Zheng (1993a; 1993b) at $T = 1300$ K. #: $\delta^{18}O_{melt}$ derived from $\delta^{18}O_{cpx}$ only; *: $\delta^{18}O_{melt}$ derived from $\delta^{18}O_{opx}$ only; &: $\delta^{18}O_{melt}$ derived from $\delta^{18}O_{cpx}$ and $\delta^{18}O_{opx}$ only. Quoted errors for oxygen isotopes are 1 s.d. based on the number of analyses (n) indicated.

Sample	Phase	$^{87}Sr/^{86}Sr$	$^{143}Nd/^{144}Nd$	$^{206}Pb/^{204}Pb$	$^{207}Pb/^{204}Pb$	$^{208}Pb/^{204}Pb$	$\delta^{18}O_{meas}$	n	$\delta^{18}O_{melt}$	n
					Ambon					
AM 3A	wr	0.721708 ± 13	0.512099 ± 5	18.963	15.675	39.097				
	bi									
AM 93A1	wr	0.711239 ± 09	0.512181 ± 7	18.886	15.678	39.128			*8.38 ± 0.25**	2
	opx						8.08 ± 0.25	2		
	bi									
	gnt						9.76 ± 0.02	2		
AM 104A1	wr	0.710509 ± 10	0.512131 ± 5	18.842	15.676	39.083			*8.12*	1
	opx						7.82	1		
					Banda Archipelago					
BA 3A	wr	0.70478	0.51287						*5.75 ± 0.05*	6
	cpx						5.33 ± 0.06	3		
	ol						4.99 ± 0.02	3		
Banda 4	wr	0.70477	0.51287	18.680	15.627	38.854			*5.78 ± 0.08*	7
	cpx						5.40 ± 0.10	4		
	ol						4.98 ± 0.06	3		
BA 6A	wr	0.7048							*5.75 ± 0.03*	7
	cpx						5.37 ± 0.02	3		
	ol						4.96 ± 0.05	4		
BA 11A2	wr	0.70478	0.51287	18.693	15.635	38.898			*5.78 ± 0.07*	6
	cpx						5.34 ± 0.07	3		
	ol						5.03 ± 0.05	3		
BA 16	wr	0.70481							*5.76 ± 0.10*	3
	cpx						5.37 ± 0.10	3		
BA 20	wr	0.70479							*5.75 ± 0.08*	6
	cpx						5.41 ± 0.09	3		
	ol						4.92 ± 0.02	3		
BA 25A	wr	0.704798 ± 12	0.512880 ± 6						*5.79 ± 0.11*	8
	cpx						5.36 ± 0.05	4		
	ol						5.05 ± 0.14	4		
BA 27A	wr	0.70481							*5.57 ± 0.11*	3
	cpx						5.18 ± 0.11	3		
BB 21A3	wr	0.70447	0.51291	18.676	15.629	38.873			*5.79 ± 0.05#*	3
	cpx						5.40 ± 0.05	3		
	ol						5.44 ± 0.03	3		
BB 28	wr	0.70459							*5.84 ± 0.30#*	2
	cpx						5.45 ± 0.30	2		
	ol						5.59 ± 0.02	2		
BN 1A	wr	0.7048							*5.69*	
	cpx						5.30	1		
BN 3A2	wr	0.70454	0.51284	18.659	15.625	38.848			*5.83 ± 0.14*	7
	cpx						5.47 ± 0.18	3		
	ol						5.02 ± 0.12	4		
BN 7A	wr	0.70476							*5.63 ± 0.04*	2
	cpx						5.24 ± 0.04	2		
BN 9A	wr	0.70478	0.51284	18.661	15.622	38.441			*5.94 ± 0.08*	3
	cpx						5.56 ± 0.11	2		
	ol						5.14	1		
					Manuk					
MA 1A	wr	0.70525	0.51273	18.754	15.647	38.973			*5.90 ± 0.11*	6
	cpx						5.54 ± 0.08	3		
	ol						5.07 ± 0.14	3		
MA 2A	wr	0.70516	0.51273						*5.91 ± 0.16*	10
	cpx						5.64 ± 0.09	4		
	opx						5.71 ± 0.08	3		
	ol						5.03 ± 0.02	3		
MA 2B	wr	0.70549	0.51277						*5.95 ± 0.02*	3
	cpx						5.56 ± 0.02	3		
MA 3C2	wr	0.70522							*5.95 ± 0.10*	7
	cpx						5.57 ± 0.10	3		
	opx						5.65 ± 0.13	4		
MA 4B	wr	0.70525							*6.08 ± 0.10*	6
	cpx						5.72 ± 0.13	3		
	opx						5.74 ± 0.07	3		

(Continued)

Table 2. Continued

Sample	Phase	$^{87}Sr/^{86}Sr$	$^{143}Nd/^{144}Nd$	$^{206}Pb/^{204}Pb$	$^{207}Pb/^{204}Pb$	$^{208}Pb/^{204}Pb$	$\delta^{18}O_{meas}$	n	$\delta^{18}O_{melt}$	n
MA 5A	wr	0.70523	0.51274	18.750	15.641	38.936			*5.97 ± 0.11*	8
	cpx						5.57 ± 0.11	4		
	opx						5.68 ± 0.13	4		
					Serua					
SE 2B	wr	0.70753	0.51259						*6.27 ± 0.06*	6
	cpx	0.707523 ± 09					5.87 ± 0.06	3		
	opx						5.97 ± 0.08	3		
SE 9A3	wr	0.70832	0.51249	19.025	15.691	39.209			*7.19 ± 0.14*[&]	8
	cpx	0.708699 ± 07					6.75 ± 0.16	5		
	opx						6.97 ± 0.06	3		
	ol						5.52 ± 0.09	3		
SE 11Sc	wr	0.70834							*6.99 ± 0.08*	6
	cpx	0.708550 ± 11					6.58 ± 0.09	3		
	opx						6.72 ± 0.09	3		
SE 17	wr	0.70838	0.51249						*7.12 ± 0.08*	7
	cpx	0.708483 ± 16					6.70 ± 0.09	4		
	opx						6.86 ± 0.04	3		
SE 21A3	wr	0.70898	0.51244	19.038	15.695	39.231			*7.12 ± 0.13*	8
	cpx	0.708853 ± 08					6.67 ± 0.17	4		
	opx						6.88 ± 0.04	4		
SE 23A	wr	0.70892							*7.06 ± 0.08*	6
	cpx	0.708880 ± 07					6.63 ± 0.05	3		
	opx						6.80 ± 0.09	3		
SE 25A	wr	0.70949	0.51240	19.019	15.694	39.226	8.01 ± 0.23	2	*7.48 ± 0.09*	6
	cpx	0.709466 ± 07					7.04 ± 0.09	3		
	opx						7.22 ± 0.09	3		
SE 26A	wr	0.70776							*6.34 ± 0.05*[&]	6
	cpx	0.707715 ± 08					5.94 ± 0.08	3		
	opx						6.04 ± 0.02	3		
	ol						5.39	1		
SE 27A	wr	0.70757	0.51261	19.084	15.696	39.270			*6.13 ± 0.11*	7
	cpx	0.707542 ± 27					5.63 ± 0.03	3		
	opx						5.91 ± 0.04	4		
SE 28A	wr	0.70752	0.51259						*6.22 ± 0.17*	7
	cpx	0.707529 ± 07					5.69 ± 0.11	3		
	opx						6.03 ± 0.11	4		
					Nila					
NI 1A1	wr	0.70770	0.51263	19.367	15.733	39.573			*5.92 ± 0.09*	7
	cpx						5.64 ± 0.08	3		
	opx						5.66 ± 0.08	4		
NI 5A	wr	0.70770							*5.80 ± 0.12*	4
	opx						5.47 ± 0.06	2		
	hbl						5.38 ± 0.19	2		
NI 5B	wr	0.70706	0.51268	19.380	15.727	39.575			*6.04*	1
	opx						5.74	1		
NI 6	wr	0.70782	0.51263						*5.89 ± 0.08*	3
	opx						5.59 ± 0.08	3		
NI 10A1	wr	0.70776	0.51259	19.321	15.731	39.552	6.21	1	*5.94 ± 0.08*	2
	cpx						5.55 ± 0.08	2		
NI 12	wr	0.70768	0.51262						*5.89 ± 0.09*	7
	cpx						5.44 ± 0.07	4		
	opx						5.66 ± 0.06	3		
NI 15I	wr	0.70698					6.76 ± 0.30	2	*5.82 ± 0.11*	5
	opx						5.52 ± 0.13	4		
	ol						5.05	1		
NI 15II	wr	0.70768					7.04 ± 0.22	2		
NI 16	wr	0.70736	0.51264	19.398	15.736	39.601	7.01	1	*5.73 ± 0.21*	5
	cpx						5.24 ± 0.33	2		
	opx						5.44 ± 0.08	2		
	ol						5.14	1		
NI 18A1/II	wr	0.70697	0.51267	19.399	15.743	39.621	6.78 ± 0.07	2	*5.84 ± 0.18*[&]	4
	cpx						5.47 ± 0.30	2		
	opx						5.52 ± 0.07	2		
	hbl						4.90	1		
NI 18A2/I	wr								*5.78*	1
	opx						5.48	1		

(Continued)

Table 2. Continued

Sample	Phase	$^{87}Sr/^{86}Sr$	$^{143}Nd/^{144}Nd$	$^{206}Pb/^{204}Pb$	$^{207}Pb/^{204}Pb$	$^{208}Pb/^{204}Pb$	$\delta^{18}O_{meas}$	n	$\delta^{18}O_{melt}$	n
					Teon					
TE 1C	wr	0.70794	0.51252	19.416	15.726	39.626			*6.48 ± 0.15*	5
	cpx						6.18	1		
	opx						6.29 ± 0.05	2		
	hbl						5.87 ± 0.06	2		
TE 5.1	wr	0.70794								
	hbl									
TE 11	wr	0.70823	0.51252						*6.24 ± 0.07*	3
	cpx						5.91	1		
	opx						5.91 ± 0.05	2		
TE 12	wr	0.70827	0.51253	19.429	15.734	39.659	8.67	1	*6.43 ± 0.15*	6
	cpx						5.97 ± 0.15	3		
	opx						6.21 ± 0.15	3		
TE 14B	wr	0.70752	0.51259	19.428	15.720	39.611			*6.26 ± 0.15*	5
	cpx						5.87 ± 0.06	2		
	opx						5.97 ± 0.20	3		
TE 15	wr	0.70732	0.51258	19.419	15.727	39.612	7.40	1	*6.18 ± 0.18*	8
	cpx						5.79 ± 0.23	5		
	opx						5.86 ± 0.09	3		
					Damar					
DA 1	wr	0.70670	0.51257	19.360	15.729	39.703			*6.03 ± 0.15*	10
	cpx						5.81 ± 0.05	2		
	opx						5.78 ± 0.10	4		
	hbl						5.44 ± 0.08	4		
DA 2	wr	0.70658							*5.94 ± 0.09*	5
	cpx						5.46 ± 0.01	2		
	opx						5.70 ± 0.02	3		
DA 3	wr	0.70660							*5.82 ± 0.14*[&]	4
	cpx						5.35 ± 0.04	2		
	opx						5.60 ± 0.18	2		
	bi						5.20	1		
DA 5	wr								*6.01 ± 0.16*[#]	2
	cpx						5.62 ± 0.16	2		
	opx						6.10 ± 0.01	2		
DA 6	wr	0.70652	0.51259							
	cpx									
	opx									
DA 8	wr	0.70699	0.51259	19.280	15.709	39.628			*5.96 ± 0.18*	4
	cpx						5.44 ± 0.11	2		
	opx						5.80 ± 0.07	2		
					Romang					
RO 2	wr	0.70849	0.51245	19.147	15.688	39.511	8.82	1		
RO 7C2	wr	0.70912							*6.13 ± 0.04*	2
	cpx						5.71	1		
	opx						5.85	1		
RO 8B	wr	0.70862	0.51246							
RO 8C6	wr	0.70917	0.51243	19.185	15.700	39.552	6.75 ± 0.10	2	*5.95*	1
	hbl						5.50	1		
RO 8E	wr	0.70923							*6.54*	1
	bi						6.02	1		

(3) Assimilation of material during fractional crystallization (AFC, DePaolo, 1981) can potentially decrease or increase $\Delta_{min-melt}$ depending on the $\delta^{18}O$ of the assimilant. Despite some Sr–Nd isotopic evidence for local effects of assimilation in the active Banda Arc (Vroon et al., 1993), there are no indications that this process has affected the $\delta^{18}O$ signatures to a large extent, as will be further discussed below. At Serua, where assimilation may have played a role, a good correspondence between Sr isotope values of clinopyroxenes and host rocks (Fig. 6) supports the assumption that AFC did not modify $\Delta_{cpx-melt}$ in a significant way.

Ranges in calculated $\delta^{18}O_{melt}$ values of lavas from the islands along the arc (Fig. 1) are from NE to SW: Ambon, 8.12–8.38‰; Banda Archipelago, 5.57–5.94‰; Manuk, 5.90–6.08‰; Serua, 6.13–7.48‰; Nila, 5.73–6.04‰; Teon, 6.18–6.48‰; Damar, 5.82–6.03‰; and Romang, 5.95–6.54‰. In contrast to Sr–Nd–Pb isotope data (Vroon et al., 1993), there is no systematic along-arc variation in $\delta^{18}O_{melt}$. Values of the active volcanoes and Romang (5.6–6.5‰) fall within the range of mantle values (Mattey et al., 1994; Eiler et al., 1996; 1997), except for the more elevated $\delta^{18}O_{melt}$ results for Serua.

Oxygen isotopes of high-K dacites and rhyolites (SiO_2 = 61.9–72.9 wt.%; Fig. 2) of Pliocene–Quaternary age (5–1 Ma, Abbot and Chamalaun, 1981; Honthaas et al., 1999) from Ambon, based on orthopyroxene phenocrysts, are the most enriched in ^{18}O ($\delta^{18}O_{melt}$ = 8.1–8.4‰). However, they may not represent primary signals. Differences in measured $\delta^{18}O$ values for orthopyroxene and garnet from sample AM93A1

Table 3. Strontium and oxygen isotopic compositions of East Indonesian sediments. $CaCO_3$, organic carbon, $^{87}Sr/^{86}Sr_{wr}$, $^{143}Nd/^{144}Nd_{wr}$ are from Vroon et al. (1995). The $^{87}Sr/^{86}Sr_{silica}$ is the Sr isotopic composition of the carbonate-free fraction (see analytical details). #: $\delta^{18}O_{wr}$ calculated assuming $\delta^{18}O_{CaCO3}$ is 29.92‰. All oxygen data are normalized to SMOW, except $\delta^{18}O_{PDB}$, which is the $\delta^{18}O$ of $CaCO_3$ normalized to PDB. *: Sr isotope data from RHBNC, others from Free University, Amsterdam.

Sample	$CaCO_3$ (wt.%)	Org. carbon (wt.%)	$^{87}Sr/^{86}Sr_{wr}$	$^{143}Nd/^{144}Nd_{wr}$	$^{87}Sr/^{86}Sr_{silica}$	$\delta^{18}O_{silica}$ SMOW	$\delta^{13}C_{CaCO_3}$ PDB	$\delta^{18}O_{CaCO_3}$ PDB	$\delta^{18}O_{CaCO_3}$ SMOW	$\delta^{18}O_{wr\ calc}$ SMOW
G5-1-002P	13.00	1.02	0.71092	0.51226	0.719238 ± 12*	19.40				20.72#
MB-1B	9.70	1.44	0.71071		0.714209 ± 07	18.70	0.99	−1.68	29.28	19.69
G5-2-24B	0.00	0.72	0.72232	0.51217	0.724650 ± 08	12.90				12.90#
G5-2-51P	16.40	1.41	0.71174	0.51221	0.726103 ± 17*	16.40	0.74	−1.34	29.53	18.48
G5-2-56P	8.60	1.32	0.71431	0.51215	0.723866 ± 06	14.50	1.00	−0.65	29.21	15.72
G5-3-69P	8.80	1.19	0.71398	0.51206	0.727675 ± 11	15.80	0.32	−2.42	28.41	16.87
G5-4-79P	8.20	1.02	0.71507	0.51214	0.723089 ± 06	17.80	−0.59	−0.62	30.27	18.78
G5-4-85P	1.00	1.40	0.71255	0.51216	0.718720 ± 06	18.40	−0.42	−0.28	30.62	18.52
G5-4-106B	2.30	0.96	0.72169	0.51217	0.727338 ± 13*	17.60				17.87#
G5-6-134B	11.60	0.38	0.73940	0.51190	0.748644 ± 06	12.90	2.38	1.72	32.69	15.11
G5-6-149P2	21.50	1.26	0.71018	0.51213	0.715073 ± 06	15.90	0.44	−0.86	30.02	18.84
G5-6-150B	41.10	1.25	0.70988	0.51210	0.715447 ± 13*	16.60	0.86	−1.22	29.65	21.84
G5-6-157B	37.70	0.98	0.71010	0.51195	0.718540 ± 13*	21.00	0.60	−1.12	29.75	24.22
DSDP262/2	24.60	0.53	0.71108	0.51218	0.715264 ± 07	14.10	0.21	−2.06	28.79	17.60
DSDP262/4	49.90		0.70971	0.51213	0.724919 ± 13*	15.60	0.48	−0.10	30.80	23.03

apparently reflects disequilibrium between these phases. This can be readily explained by the xenocrystic nature of the garnet, as the sample contains abundant thermometamorphic xenocrysts that are characterized by Al-rich assemblages including cordierite, Al-spinel, and sillimanite. Petrographic observations indicate that high loads of xenocrysts are a common feature in the volcanics of Ambon (Van Bergen et al., 1989; Honthaas et al., 1999). Hence, the elevated $\delta^{18}O$ value inferred here for the bulk rocks could reflect incomplete assimilation of high-grade metamorphic basement rocks.

4.2.2. Comparison with conventional whole-rock data

Compared with conventional $\delta^{18}O_{wr}$ data of the Banda Arc (Magaritz et al., 1978) the new $\delta^{18}O_{melt}$ laser fluorination data are up to 2‰ lower (Fig. 7). In order to verify this discrepancy we have analyzed 10 of our samples for whole-rock $\delta^{18}O$ as well (Table 2). The results show similar differences with the laser fluorination phenocryst data and are comparable with the findings of Magaritz et al. (1978).

If mineral–liquid disequilibrium (e.g., as a result of AFC) can be discarded (as supported by the correspondence between Sr-isotope data of cpx and whole rock in the case of Serua, Fig. 6), the observed differences might be attributed to post-emplacement alteration. Other studies have corrected whole-rock oxygen-isotope composition for secondary water take-up after eruption, based on LOI or H_2O contents (Taylor et al., 1984; Ferrara et al., 1985; 1986; Davidson and Harmon, 1989; Ellam and Harmon, 1990). However, absence of a correlation between LOI and the difference between $\delta^{18}O_{wr}$ and $\delta^{18}O_{melt}$ in our samples (Fig. 7) makes such a recalculation procedure dubious, if post-eruptive water take-up and alteration would have changed original values at all. Moreover, the laser fluorination results yield far less spread in $\delta^{18}O$ values, and form a more coherent data set.

It is noteworthy that the parallel trends of the whole rock and LF data are observed in the Lesser Antilles data set as well (Fig. 8). The offset between the whole rock and LF $\delta^{18}O$ data is similar, ca. 1–2‰. Up to 1‰ of the shift observed in these data sets can be explained by differences in melt–mineral fractionation for clinopyroxene phenocrysts and a plagioclase-dominated ground mass crystallizing at 1000°C (e.g., Zheng, 1993a). The remaining offset for some samples of <1‰ could be a result of post-eruptive alteration, or could be an artefact of low yields of oxygen extracted from Fe-rich minerals, which make up approximately 5% of the ground mass, during whole-rock analysis.

We conclude that data from phenocrysts are more appropriate for modelling of *magmatic* oxygen-isotope signatures than the present and earlier whole-rock data. Hence, in contrast to earlier views, the volcanic rocks of the active Banda Arc are characterized by *mantle-like* $\delta^{18}O$, despite the evidence for involvement of subducted sediment.

4.2.3. Comparison with other island arcs

Available whole-rock $\delta^{18}O$ data for active volcanoes in the Java and Adonara–Pantar sectors of the Sunda Arc (see Fig. 8) range between mantle values (~5.5‰) and 8‰ (Van Bergen et al., 1992; Stolz et al., 1988; Edwards et al., 1991; 1994; Harmon and Gerbe, 1992; Macpherson, 1994). Volcanics from Wetar, in the extinct sector separating the Banda Arc from the Sunda Arc, show an extreme spread in $\delta^{18}O$ between 6.2 and 18.1‰, and a covariation with Nd and Sr isotopes (McCulloch et al., 1982). High $\delta^{18}O$ values (7.8–16.7‰) also characterize the Pliocene volcanics of Ambon (Magaritz et al., 1978).

The Banda Arc $\delta^{18}O_{melt}$ signatures are comparable with whole-rock and plagioclase values of 5.5–6.6‰ that were found in the Mariana–Izu-Volcano Arc (Ito and Stern, 1985; Woodhead et al., 1987) and the Aleutians (Singer et al., 1992), whereas they are generally lower than $\delta^{18}O_{wr}$ values reported for the Lesser Antilles Arc (5.5–14‰, Davidson, 1985; Davidson and Harmon, 1989; Smith et al., 1996; Thirlwall et al., 1996) and the Eolian Arc (6.1–8.5‰, Ellam and Harmon, 1990). Harmon and Hoefs (1995) reported a conventional $\delta^{18}O_{wr}$ range of 5.3–7.5 ‰ with an average of 6.1 ± 1.1‰ for oceanic arc basalts, which they had filtered for secondary, post-

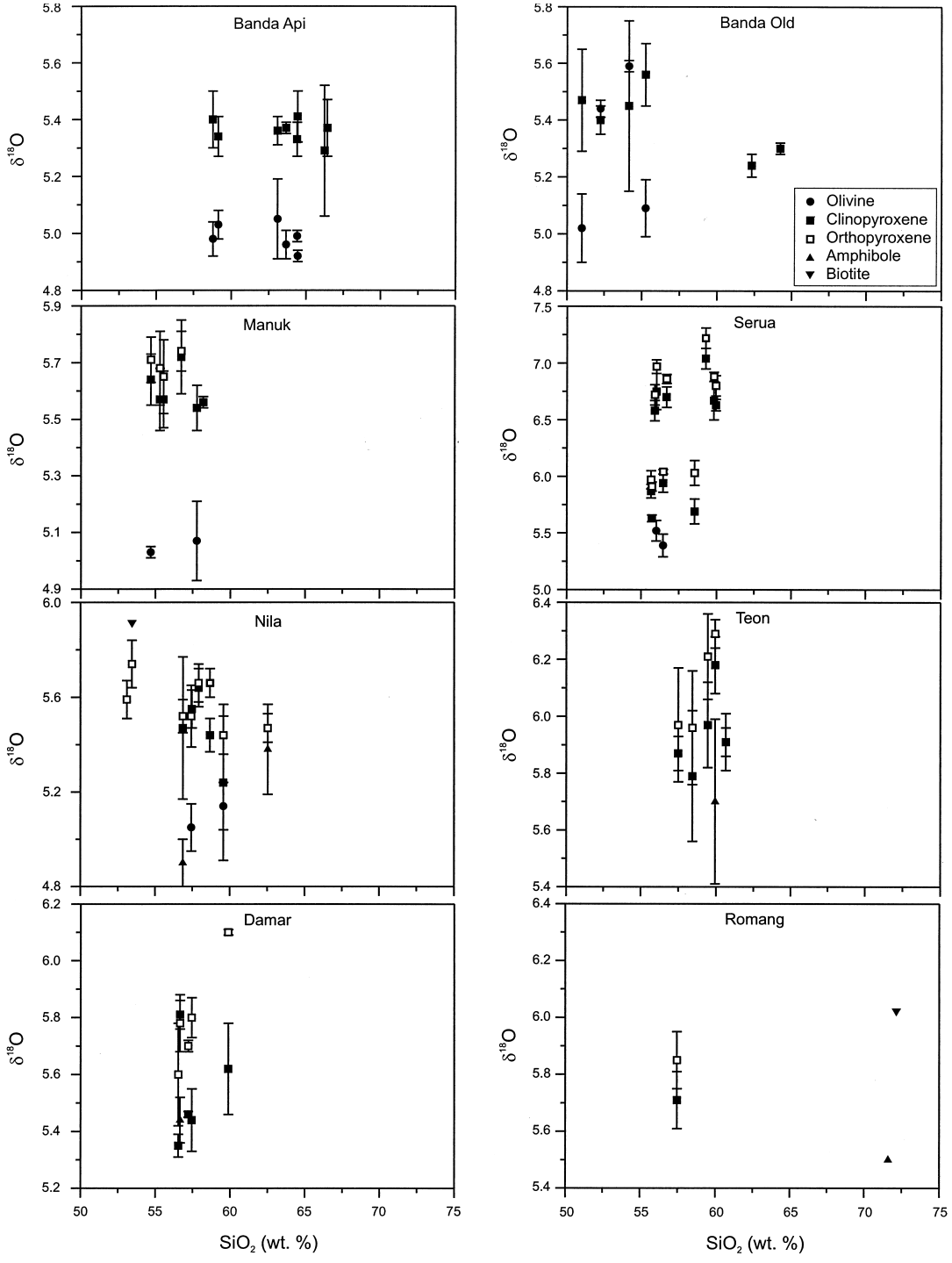

Fig. 4. SiO_2 versus $\delta^{18}O$ of measured minerals for Banda Arc volcanic rocks. Note $\delta^{18}O$ scale difference for Serua and Nila. Error bars are 1 s.d. See text for discussion.

depositional alteration. The $\delta^{18}O_{melt}$ range in the Banda Arc (5.57–7.48, excluding Ambon) presented here overlaps with the oceanic-arc range, but with less variation (average 6.10 ± 0.44‰).

Recent LF results on olivines from the Mariana, Vanuatu–Fiji, and South Sandwich Arcs (Eiler et al., 2000) allow a direct comparison between the oxygen-isotope signatures of the Banda Arc lavas (Banda Archipelago, Manuk, Serua, Nila) and basalts from typical oceanic island arcs. This shows that there is complete overlap between Banda Arc values ($\delta^{18}O_{olivine}$ = 4.92–5.52) and the other arcs ($\delta^{18}O_{olivine}$ = 4.85–5.78), despite the more evolved character of lavas from the Banda Arc. A similar overlap exists with LF data from basalts in the Kermadec Arc, for which Macpherson et al. (1998) reported values of $\delta^{18}O_{olivine}$ = 4.83–5.47.

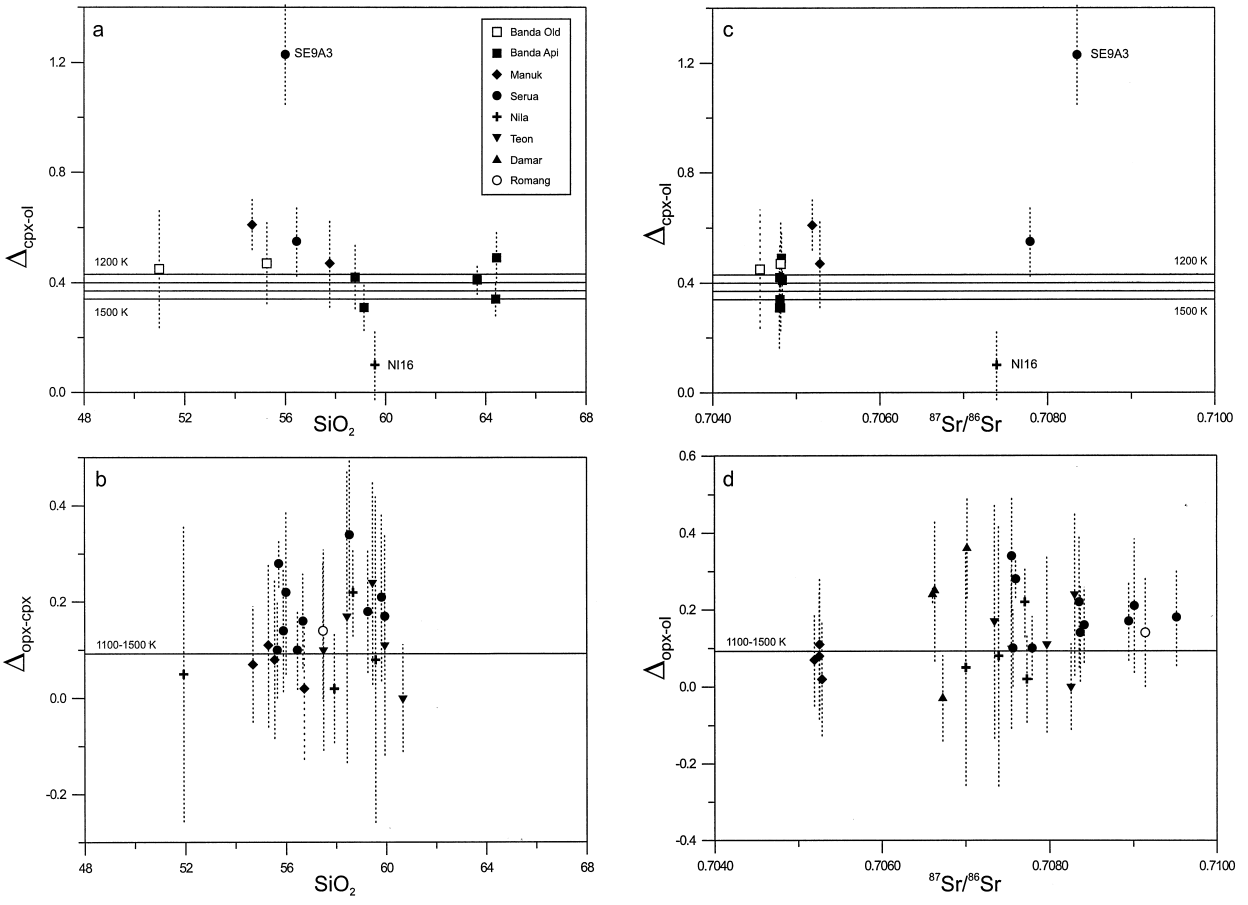

Fig. 5. (a)–(d) Δ_{cpx-ol} and $\Delta_{opx-cpx}$ versus SiO_2 (a) and (b) and $^{87}Sr/^{86}Sr$ (c) and (d). Experimental values of Δ_{cpx-ol} at different temperatures (1200–1500 K) are from Kalamarides (1986); the theoretical $\Delta_{opx-cpx}$ value from Zheng (1993a) is virtually constant for 1100–1500 K. Note that most opx–cpx pairs are in equilibrium. In contrast, two of the ol–cpx pairs from Serua (SE9A3) and Nila (NI16) are clearly out of equilibrium. Bars are based on propagated analytical errors. Samples BB21A3 and BB28 (Table 2) are not shown because they contain altered olivine.

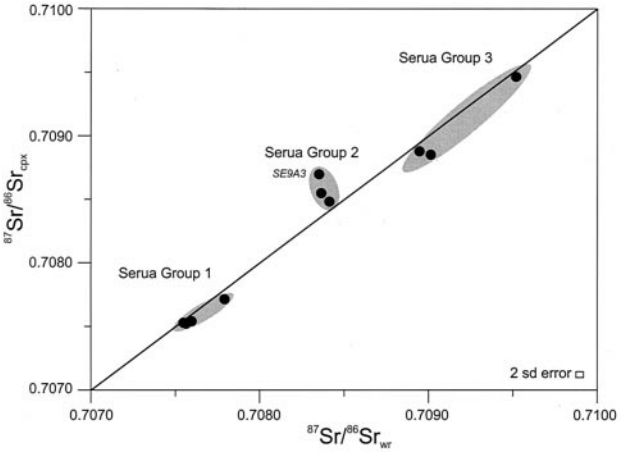

Fig. 6. Plot of $^{87}Sr/^{86}Sr$ ratios for Serua lavas, suggesting equilibrium between clinopyroxene and bulk magma in three distinct groups. The largest deviation in a sample from group 2 (SE9A3) corresponds with the observed Δ_{cpx-ol} disequilibrium in oxygen isotopes (see Fig. 5).

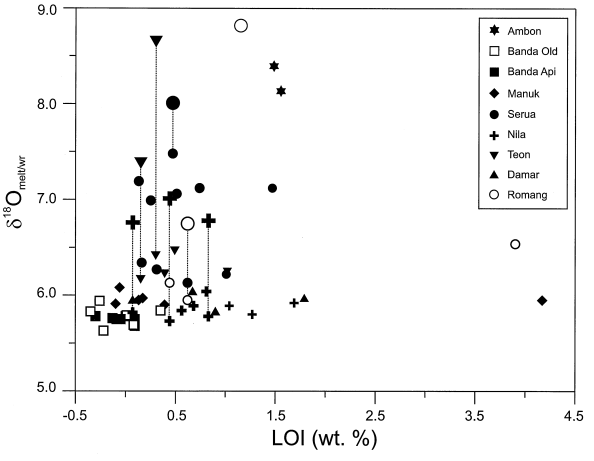

Fig. 7. LOI (Loss on Ignition) versus $\delta^{18}O_{melt}$ (small symbols) and $\delta^{18}O_{wr}$ (large symbols) for the Banda Arc suites. Data points for the same samples are connected by tie lines. Absence of a correlation between LOI and $\delta^{18}O_{melt}$ or $\delta^{18}O_{wr}$ and $\delta^{18}O_{melt}$ precludes systematic changes in $\delta^{18}O_{wr}$ as a result of secondary water take-up or alteration (cf. Ferrara et al., 1986). Note that the $\delta^{18}O_{wr}$ values have variable offsets compared to $\delta^{18}O_{melt}$ of the same sample, suggesting that any secondary changes may not be uniform and therefore no simple correction can be applied.

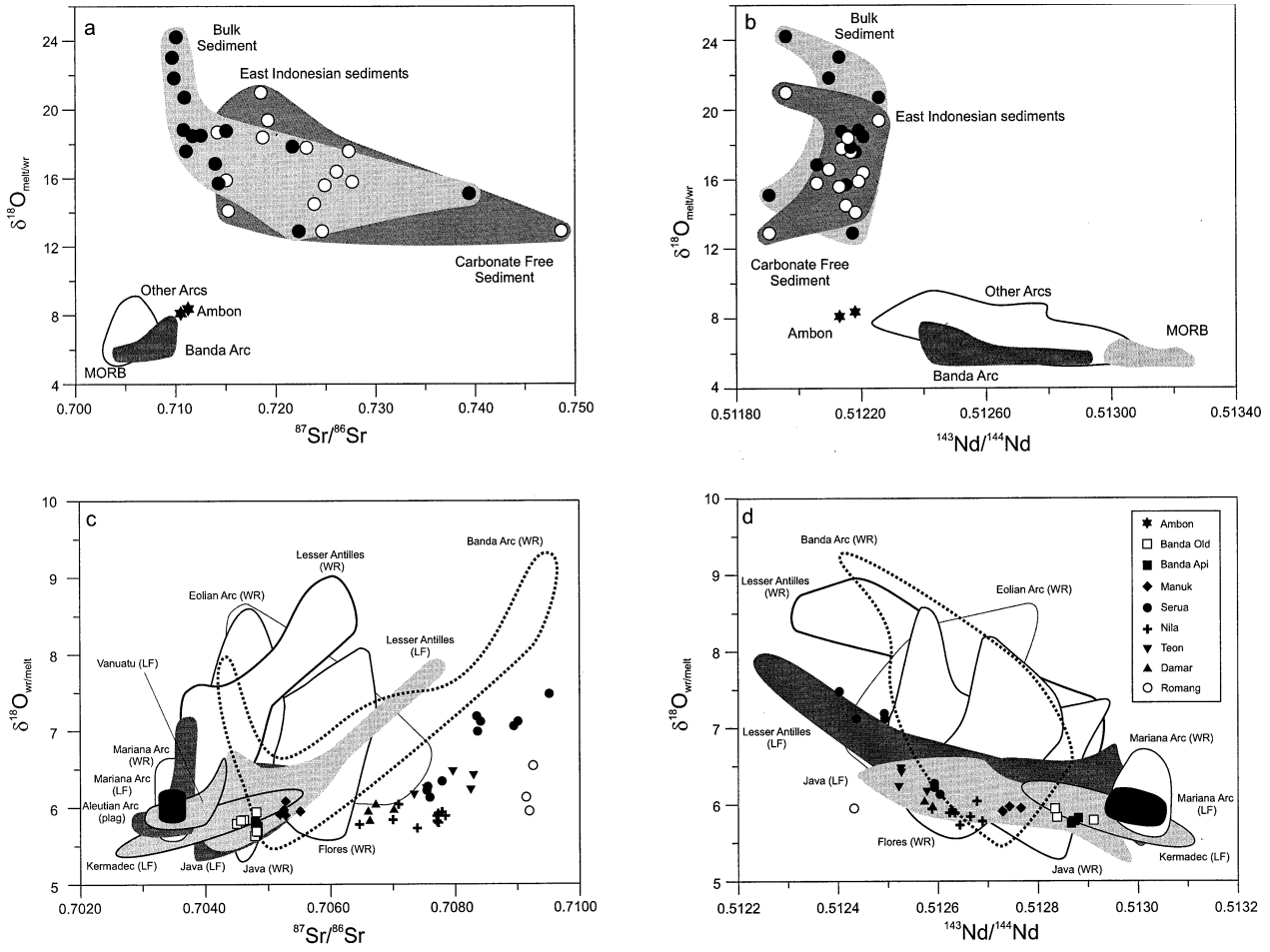

Fig. 8. (a)–(d) $\delta^{18}O$ versus $^{87}Sr/^{86}Sr$ [(a) overview; (c) detail] and $^{143}Nd/^{144}Nd$ [(b) overview; (d) detail] diagrams for Banda Arc lavas compared with $\delta^{18}O_{wr}$ of the Banda Arc (Magaritz et al., 1978; this study), the Eolian Arc (Ellam and Harmon, 1990), the Lesser Antilles Arc (wr: Davidson and Harmon, 1989; Thirlwall et al., 1996; LF: Smith et al., 1996; Thirlwall et al., 1996), the Mariana Arc (wr: Ito and Stern, 1985; Woodhead et al., 1987; LF: Eiler et al., 2000), Vanuatu (LF: Eiler et al., 2000), the Java sector of the Sunda Arc (wr: Harmon and Gerbe, 1992, Edwards, 1991; 1994, LF: Macpherson, 1994), the Flores sector of the Sunda Arc (Stolz et al., 1988; Edwards, 1991; Van Bergen et al., 1992), the Aleutian Arc (plag: Singer et al., 1992) and the Kermadec Arc (LF: Macpherson et al., 1998) and East Indonesian sediments. LF data have been converted to melt values according to $\delta^{18}O_{melt} = \delta^{18}O_{cpx} + 0.39$ and $\delta^{18}O_{melt} = \delta^{18}O_{ol} + 0.79$. Altered MORB form Staudigel et al. (1995). Note that the $\delta^{18}O_{melt}$ values of Banda Arc samples are significantly lower than the $\delta^{18}O_{wr}$ results. Similar differences between $\delta^{18}O_{wr}$ and calculated $\delta^{18}O_{melt}$ (LF data) can also be observed in the Lesser Antilles and Java. Abbreviations: BS = average bulk sediment; CFS = average carbonate free sediment (Table 4).

4.3. Oxygen Isotopic Composition of East Indonesian Sediments

Table 3 presents oxygen isotope results for sediments from East Indonesia (for locations see Fig. 1), of which Sr–Nd–Pb and trace elements were reported in Vroon et al. (1995). The carbonate fraction has a near constant $\delta^{18}O_{SMOW}$ of 29.9 ± 0.9‰, similar to late Quaternary planktonic foraminifera from the Banda Sea region ($\delta^{18}O_{SMOW}$ = 27.8–29.9‰, Ahmad et al., 1995). The silicate-fraction $\delta^{18}O$ varies between 12.9 and 21.0‰, and does not show a simple relationship with Sr–Nd isotopes (Fig. 8). Calculated $\delta^{18}O_{wr}$ values (15.1–24.2‰) are similar to whole-rock data of sediments from the Lesser Antilles (wr: 19.6–20.8‰, Davidson et al., 1987) and Pacific Ocean (wr: 16.0–30.1‰, Woodhead et al., 1987), but they are higher than data for the volcaniclastic sediments of the Kermadec Ridge and Trench (silicate fraction: 8.0–13.9‰, Macpherson et al., 1998). The average oxygen-isotope composition of the silicate fraction (16.5 ± 2.4‰) compares well with a Triassic shale from the Timor Trough (Fig. 1) which has $\delta^{18}O$ = 16.4‰ (McCulloch et al., 1982). Sr isotopic ratios determined on the same silicate fraction are all radiogenic and average around 0.7229 ± 86 (Table 3), which is consistent with a large fraction of old continental material.

5. DISCUSSION

5.1. Involvement of Subduction of Continental Material

The islands of the Banda Archipelago, Manuk, Nila, Damar, and Romang (Fig. 1) have low $\delta^{18}O_{melt}$ (5.5–5.9‰), whereas Sr–Nd–Pb–Hf–He and U-series systematics all point to signif-

Table 4. End-member compositions used in mixing calculations. Depleted MORB mantle: oxygen isotopes from Harmon and Hoefs (1995); average Sr and Nd isotope ratios from a compilation of Indian–MORB data in Vroon et al. (1993); trace-element data: GERM (http://pacer2.ucsd.edu/germ/). Average carbonate-free (CF) and bulk-sediment compositions were calculated from samples for which oxygen-isotope data are available only (Table 3), using data from Vroon et al. (1995). The fluid end-member was calculated with carbonate-free sediment and the mobility data for amphibolite dehydration of Kogiso et al. (1997), assuming that the mobility of Zr equals that of Nb.

	Depleted MORB mantle	Arc magma (Serua type)	Bulk sediment (BS)	Carbonate free sediment (CFS)	Fluid from CFS	Sediment G5-6-134B	Ambon Arc crust
$\delta^{18}O$ (‰)	5.70	5.90	18.7	16.5	16.5	12.9	9.8
O (wt.%)	43.8	44.2	50.2	50.2	88.9	50.2	50.2
$^{87}Sr/^{86}Sr$	0.7026	0.7075	0.7156	0.7229	0.7258		
$^{143}Nd/^{144}Nd$	0.51310	0.51260	0.51212	0.51212	0.51212	0.51190	0.51190
Sr (ppm)	12.94	350	450	180	73.4		
Nd (ppm)	0.73	14	24.2	27	8.34	27	27
Nb (ppm)	0.11		9.75	10.6	0.38		
Zr (ppm)	6.20		134	147	5.29		

icant contributions (1–5%) of subducted continental material (SCM) to magma sources (Whitford et al., 1977; 1981; Whitford and Jezek, 1979; Gill and Williams, 1990; Hilton et al., 1989; 1992; Vroon et al., 1993; 1995; 1998). Strong evidence for source contamination is provided by parallel Nd–Pb isotopic trends in volcanic rocks and sediments along the East Sunda–Banda Arc (Vroon et al., 1993; 1995; Van Bergen et al., 1993). Hence, the overall low $\delta^{18}O$ signatures most likely represent source characteristics and will be discussed here first. The relatively high $\delta^{18}O$ values observed in some of the individual centers will be investigated in more detail, given independent evidence for arc−crust assimilation (Vroon et al., 1993).

5.1.1. Single subduction component mixing models

The dominant mantle end-member in the Banda Sea area is thought to be a depleted MORB-type mantle (Stolz et al., 1990; Vroon, 1992; Vroon et al., 1993; Hoogewerff et al., 1997). Although indications exist for involvement of enriched mantle types as well (e.g., Van Bergen et al., 1992; Vroon et al., 1993), this would not affect the $\delta^{18}O$ systematics inferred here, since there is probably little $\delta^{18}O$ variation among different mantle domains (Mattey et al., 1994; Eiler et al., 1996; 1997). The depleted MORB end-member given in Table 4, represents a typical Indian–MORB mantle.

The SCM end-member is well characterized for radiogenic isotopes, oxygen isotopes, and trace elements (Table 4) by the composition of recent Australian shelf sediments (Vroon, 1992; Vroon et al., 1995). Although all of the sampled sediments are young (<3 Ma), their provenance areas have changed little since the Cretaceous, and it is appropriate to assume that the sediments/crust currently involved in magma genesis have a similar geochemical composition (see Vroon et al., 1995 for more details). Because of a significant difference in strontium and oxygen isotopes between carbonate-rich and carbonate-free sediments, we have distinguished between these sedimentary end-members in the mixing calculations (Table 4).

The composition of the bulk-sediment end-member is assumed to be the average of the sediment data reported in Vroon et al. (1995). Cenozoic sediments in ODP site 765 are $CaCO_3$-rich (57.5%), whereas older sediments contain 9.8% $CaCO_3$ (Plank and Ludden, 1992). For simplicity, carbonate-free sediment is used here as an approximation of the subducted continental material (SCM), since minor amounts of carbonate would not affect the final conclusions.

Figure 9 shows simple models for bulk mixing between Indian–MORB mantle and the SCM end-members, represented by carbonate-free and bulk sediment. As a first approximation, all islands (except Serua) can be fitted with bulk-mixing curves (James, 1981). The amounts of bulk SCM tend to increase along the arc from $<1\%$ in the Banda Archipelago to $>3\%$ in Romang. These systematics are similar to the findings in bulk-mixing models for Sr–Nd–Pb–He isotopes (e.g., Hilton et al., 1991; Vroon et al., 1993), and appear to reflect an increase in SCM contributions towards the arc sector near Timor, where the Australian continent collided first. Variations in the compositions of the mantle and sediment end-members would not significantly change the position of the mixing curves or the percentages of added SCM. Magaritz et al. (1978) used a similar bulk-mixing approach to interpret the oxygen isotope systematics in terms of source contamination by continent-derived sediments, but the principal difference is that these authors invoked the model to explain relatively high $\delta^{18}O$ values, whereas our conclusion is that low $\delta^{18}O$ is more consistent with such a SCM contribution. The ratio of Sr concentrations in the mantle and sedimentary end-members of 1:3 used by Magaritz et al. (1978) differs from end-member data defined here (1:20). Our model thus generates a stronger curvature of mixing lines, which readily explains the discrepancy.

5.1.2. Refined models

Although the above bulk-mixing model is capable of explaining the variation of oxygen and radiogenic isotopes in the Banda Arc, it is inconsistent with the observed trace-element signatures. This is illustrated in Fig. 10, where bulk-mixing curves in Zr/Nb-$\delta^{18}O$ space do not fit for the southern Banda Arc centers.

As an alternative, we have modelled a scenario where SCM-derived melt is mixed with a depleted MORB mantle. We assumed that the SCM component melts to a large degree (25%), as predicted by experiments (Johnson and Plank, 1999) and Lu/Hf systematics (Vroon et al., 1998). The proportions of minerals present in the source were calculated by minimizing root-mean-square difference between the calculated and ob-

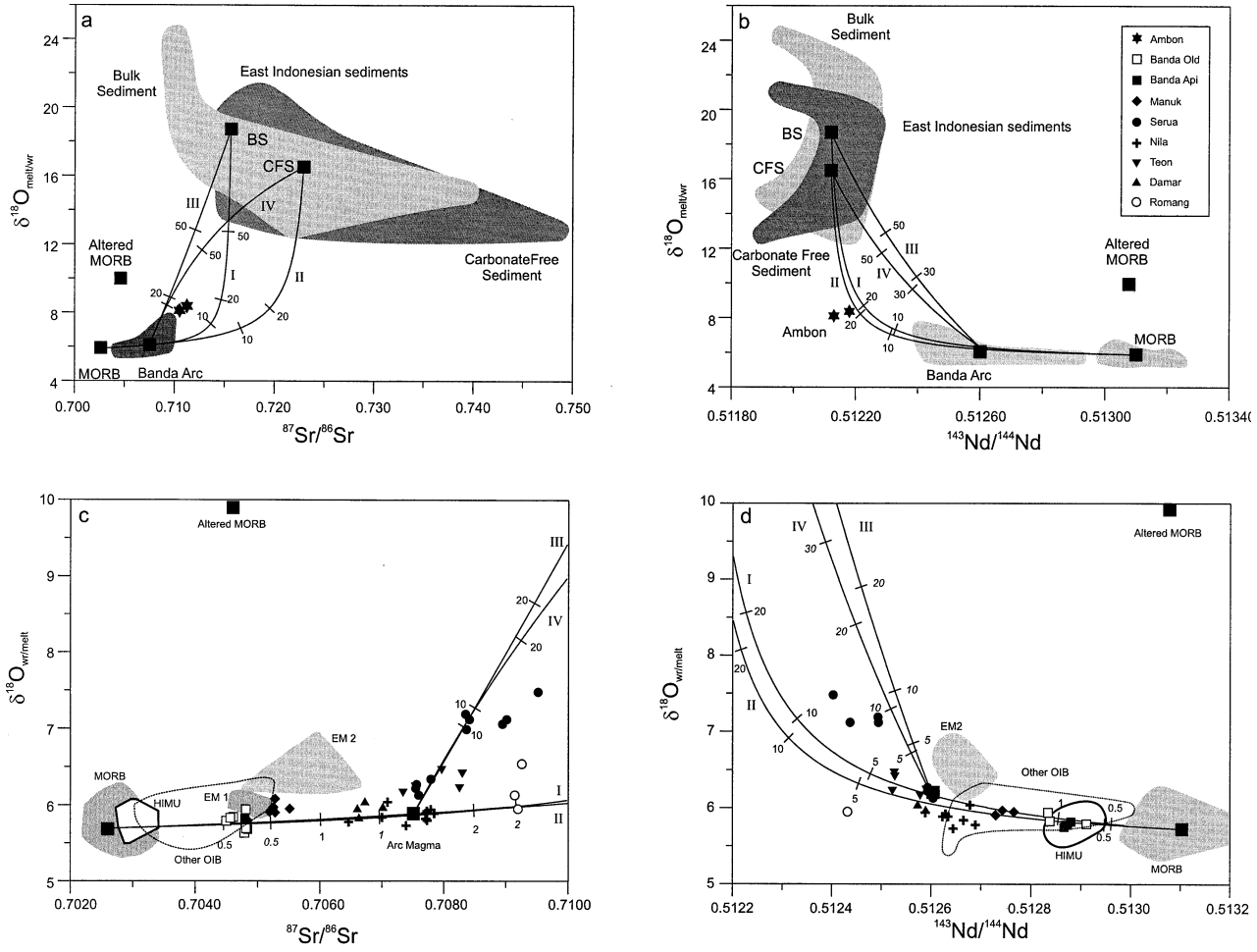

Fig. 9. (a)–(d) Banda Arc data plotted in diagrams similar to Fig. 8, showing bulk-mixing models for MORB-sediment and arc magma-sediment combinations, and a comparison with whole-rock and olivine laser-fluorination data (converted to $\delta^{18}O_{melt}$ values with $\Delta_{melt-ol} = 0.89$) from MORB (wr: Ito et al., 1987; LF: Eiler et al., 1997) and OIB (HIMU, EM 1, EM 2, and other OIB; LF: Eiler et al., 1996; 1997). End-member compositions are given in Table 4. Curves shown: I, MORB source–Bulk sediment (BS); II, MORB source–carbonate-free sediment (CFS); III, arc magma–BS; IV, arc magma–CFS. See text for discussion.

served major-element composition of average east Indonesian sediments (Vroon et al., 1995), assuming that phlogopite, quartz, clinopyroxene, and garnet are the principal mineral components. All TiO_2 was assumed to be stored in rutile, and all Zr in zircon (e.g., Vroon et al., 1998). The resulting mineral contents and distribution coefficients used are given in the caption of Fig. 10. The SCM melt model yields a good fit for all of the Banda Arc centers (except Serua, Fig. 10). The amounts of melt added to depleted MORB range between 0.1 and 10% and are slightly smaller than in the case of bulk mixing.

Similar relations can be derived from a $^{143}Nd/^{144}Nd$-$\delta^{18}O$ diagram (Fig. 11), which also shows that the Banda Arc plots on a mixing curve between depleted MORB mantle and melt derived from SCM. Calculated percentages of added melt are lower than in the Zr/Nb-$\delta^{18}O$ model (Fig. 10), particularly for the southern Banda Arc (Nila–Teon–Damar–Romang). However, it should be noted that the Zr/Nb ratio is highly sensitive to the starting composition of SCM and input parameters adopted. Models based on strontium isotopes are ill constraint because of the large range in $^{87}Sr/^{86}Sr$ ratios and Sr contents of the sediments [cf. Fig. 8(a)].

Despite uncertainties in melting models and parameters, the conclusions from these examples seem valid for large ranges in source composition, melting degree, and distribution coefficients. The most important point to stress is that fluid components are inadequate to generate the oxygen-isotope signatures (Figs. 10 and 11), although involvement of a fluid in shallow parts of the subduction zone of the East Sunda–Banda Arc has been demonstrated for the low-K volcanoes of the Banda Archipelago and Werung in the East Sunda Arc (Vroon et al., 1993; Hoogewerff et al., 1997). In other cases any fluid signature may have been largely swamped by the SCM melt component.

We have also tested mantle–magma interaction models, similar to that originally proposed by Kelemen et al. (1990) to explain the LILE/HFSE signatures of island–arc volcanic rocks. Figures 10 and 11 show that $\delta^{18}O$ values of ascending

SCM melts that interact with a surrounding lherzolitic mantle wedge can obtain mantle values, whereas incompatible trace element ratios (e.g., Zr/Nb) and Nd isotopes still record the original SCM melt signatures. The strong curvature of the melt–mantle interaction line reflects differences in concentrations and distribution coefficients between oxygen and incompatible trace elements. Since mantle periodotite is depleted in incompatible trace elements compared to the ascending melt and distribution coefficients are low, the effect of mantle assimilation on incompatible trace element ratios (e.g., Th/Nb) is limited. On the other hand, a more rapid equilibration between SCM melt and mantle material can be expected for oxygen, given the low concentration difference and the distribution coefficient being close to unity. Mantle AFC could have played a role, but the effects are too small to distinguish between mantle AFC and mixing SCM melt with a depleted MORB source (Figs. 10 and 11).

Table 5 summarizes our findings for source mixing in the Banda Arc compared with evidence in other island arcs for which LF oxygen isotope data are available. The Banda Arc clearly differs from other settings in the nature of the subduction component (dominated by SCM melt) and in the calculated contribution of up to 1.5% (for the SW part of the arc), taking $^{143}Nd/^{144}Nd$-$\delta^{18}O$ as a reference. Mixing with bulk sediment, as postulated for Grenada, Lesser Antilles (Thirlwall et al., 1996) would require up to 2%. Oxygen–isotope systematics in other island arcs have been explained in terms of a subduction component dominated by aqueous fluids (Smith et al., 1996; Macpherson et al., 1998; Eiler et al., 2000).

Eiler et al. (2000) reported correlations between oxygen isotopes of olivines from oceanic island–arc lavas and parameters indicating the degree of partial melting (e.g., $TiO_{2(8.0)}$ and the Yb/Sc ratio). They attributed these relations to fluid-fluxed melting of a peridotite source, whereby increasing $\delta^{18}O$ would be associated with an enhanced degree of melting. Fluid and melt modelling led Eiler et al. (2000) to conclude that slab derived aqueous fluid plays a dominant role in island arcs. In this respect, it is of interest to note that $\delta^{18}O_{ol}$ and $TiO_{2(8.0)}$ are inversely correlated in the Banda Arc (Fig. 12), if we discard Serua (assimilation, see below) and Teon (insufficient data for a reliable Mg–TiO_2 regression). The observed Banda Arc trend shows that melts derived from subducted continental material in a continent–arc collision setting are capable of generating source mixing variations that are similar to those predicted by the Eiler et al. fluid-fluxed models for oceanic island arcs. The decrease in TiO_2 can be explained by the relatively low TiO_2 content of the slab component, which reflects titanium retention by rutile in the sediment residue (e.g., Vroon et al., 1998).

In summary, the subduction component in the Banda Arc is dominated by a melt derived from SCM. The SCM melt component is small in the NE part of the Banda Arc: 0.1–0.5%, and significantly larger in the SW: 1–1.5%. Magma–mantle wedge interaction could enhance the low $\delta^{18}O$ in the Banda Arc, but it is difficult to test with the oxygen–radiogenic isotopes alone. The correlation of $\delta^{18}O$ with melting parameters such as those found by Eiler et al. (2000) is also displayed by the Banda Arc volcanic centers. Therefore, fluid-fluxed melting is not the only mechanism to generate these correlations.

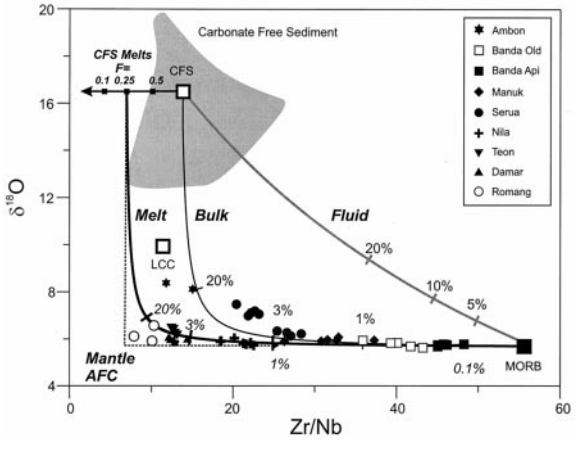

Fig. 10. Zr/Nb versus $\delta^{18}O_{melt}$ diagram showing mixing of depleted MORB mantle with carbonate-free sediment (CFS) and with CFS-derived fluid or melt. End-member compositions are given in Table 4. The melt composition was calculated assuming batch melting (melt fraction F = 0.25) of a CFS source. Mineral proportions in the CFS source were approximated by minimizing the root-mean-square difference between the calculated and observed major-element composition of average east Indonesian sediments for an assumed mineral assemblage (Vroon et al., 1995): cpx = 35.8%; garnet = 14.5%; coesite = 16.9%; phlogopite = 31.7%, rutile = 1.0%, and zircon = 0.1%. Bulk distribution coefficients: D_{Nb} = 0.61 and D_{Zr} = 1.15 (based on the calculated mineral contents in the source). The curve for mantle AFC represents a magma–mantle interaction model after Kelemen (1990), in which the F = 0.25 melt derived from CFS reacts with depleted MORB mantle (Table 4). Parameters: r = 0.9999, D_O = 1.0, D_{Nb} = 0.1, and D_{Zr} = 0.2. LCC: Lower continental crust (Rudnick and Fountain, 1995). See text for discussion.

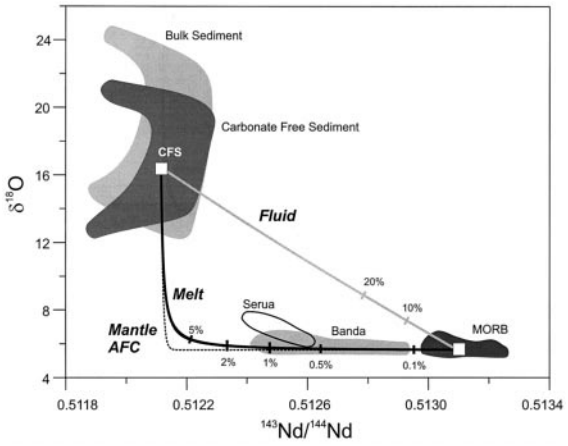

Fig. 11. $^{143}Nd/^{144}Nd$ versus $\delta^{18}O$ diagram showing mixing between depleted MORB mantle and fluid or melt derived from subducted continental material. End-member compositions are given in Table 4. Melt model and source compositions as in Fig. 10, with bulk distribution coefficient: D_{Nd} = 0.095. The curve for mantle AFC represents a magma–mantle interaction model after Kelemen (1990), in which the F = 0.25 melt derived from CFS reacts with depleted MORB mantle. Parameters: r = 0.9999, D_O = 1.0 and D_{Nd} = 0.1. Note that the model predicts that survival of high $\delta^{18}O$ (>6.5‰) signatures is highly unlikely.

5.3. High $\delta^{18}O$: Evidence for Assimilation of Arc Crust?

5.3.1. Serua

Many oxygen-isotopes studies have shown that assimilation of crustal material is an important process capable of generat-

Table 5. Banda Arc subduction component compared with other island arcs for which laser fluorination oxygen isotope data are available. See text for discussion.

Arc	Nature of subduction component	Contribution subduction component	Based on $\delta^{18}O$ in combination with	Reference
Banda NE	Sediment melt + bulk	0.1–0.5%	$^{143}Nd/^{144}Nd$	This study
Banda SW	Sediment melt + bulk	1–1.5% (10%)	$^{143}Nd/^{144}Nd$	This study
Kermadec	95:5 fluid altered oceanic crust-sediment	0.5–1.5%	$^{143}Nd/^{144}Nd$–$^{87}Sr/^{86}Sr$	Macpherson et al., 1998
Lesser Antilles, Grenada	Bulk sediment	0.2–2.0%	$^{143}Nd/^{144}Nd$–$^{87}Sr/^{86}Sr$	Thirlwall et al., 1996
Lesser Antilles, Bequia	Fluid	1.0–4.0%	$^{87}Sr/^{86}Sr$	Smith et al., 1996
Vanuatu	Fluid	1.0–2.0%	$TiO_{2(8.0)}$	Eiler et al., 2000
South Sandwich	Fluid	<0.5%	$TiO_{2(8.0)}$	Eiler et al., 2000
Mariana	Fluid	<0.5%	$TiO_{2(8.0)}$	Eiler et al., 2000

ing elevated $\delta^{18}O$ signatures in arc volcanics (Davidson and Harmon, 1989; Ellam et al., 1990; Singer et al., 1992; Smith et al., 1996; Macpherson et al., 1998). In these studies, the evidence for assimilation is generally based on correlations between radiogenic isotopes, oxygen isotopes, and/or differentiation indices (e.g., SiO_2, Mg number). Some of the within-suite SiO_2–$^{87}Sr/^{86}Sr$ relations in the Banda Arc are consistent with AFC involving a crustal component, but similar systematics are not observed in the SiO_2-$\delta^{18}O$ plot, as most of the oxygen-isotope data even remain below reasonable trends for crystal fractionation [Fig. 13(a)].

The lavas of Serua form an exception and combine a large variation in $\delta^{18}O$, $^{87}Sr/^{86}Sr$ and $^{143}Nd/^{144}Nd$ values with a limited range in major and trace element contents (Fig. 2). In detail, three Serua groups can be distinguished (e.g., Fig. 6).

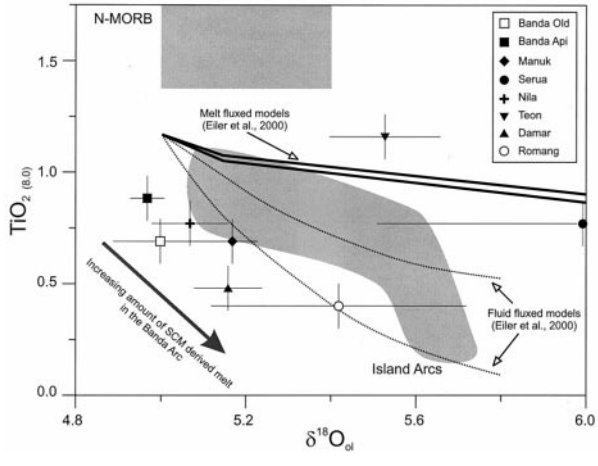

Fig. 12. $\delta^{18}O_{ol}$ versus $TiO_{2(8.0)}$ modified after Eiler et al. (2000). Average $\delta^{18}O_{melt}$ values of the Banda Arc volcanic centers (Table 2) have been recalculated to $\delta^{18}O_{ol}$ ($\delta^{18}O_{ol} = \delta^{18}O_{melt} - 0.79$). $TiO_{2(8.0)}$ is the TiO_2 content at 8% MgO using a regression of MgO–TiO_2 data for one volcanic suite (see Eiler et al., 2000 for details). TiO_2 and MgO data from Vroon (1992). Only samples with MgO > 3% have been included in the regressions. Error bars indicate 1 s.d. for $\delta^{18}O_{ol}$ and an estimated 10% error for the $TiO_{2(8.0)}$ values. The fields of N-MORB and other island arcs and the melting models are from Eiler et al. (2000). Note that the Banda Arc centers display a similar negative correlation between $\delta^{18}O_{ol}$ and $TiO_{2(8.0)}$ as other island arcs if we discard Serua and Teon. See text for discussion.

Group 1 is characterized by low $\delta^{18}O_{melt}$ (6.13–6.34) and relatively low $^{87}Sr/^{86}Sr$ (0.7075–0.7078) and high $^{143}Nd/^{144}Nd$ ratios; group 2 has intermediate values for $\delta^{18}O_{melt}$ (6.99–7.19) and radiogenic isotopes, whereas group 3 has the highest $\delta^{18}O_{melt}$ (7.06–7.48), highest $^{87}Sr/^{86}Sr$ (0.7089–0.7095), and lowest $^{143}Nd/^{144}Nd$ ratios. The isotopic characteristics of group 1 can be readily explained by the addition of SCM to the sub-arc mantle, following the general source-contamination pattern of the Banda Arc. The high $\delta^{18}O_{melt}$ values in group 3 probably reflect assimilation of arc-crust material. This is consistent with bulk models showing that a combination of source contamination and addition of local sediments to uprising magmas is capable of producing some of the observed Sr–Nd isotopic signatures of Serua, as discussed in Vroon et al. (1993). The lavas of group 2 most likely represent mixtures produced by back-mixing of group 3 magma with freshly arriving batches of uncontaminated group 1 magma. This is supported by the observed isotopic disequilibrium features in group 2. The low $\delta^{18}O_{ol}$ value of sample SE9A3 and the large Δ_{cpx-ol} (Fig. 5) suggest that the olivine originate from group 1 type magma. Furthermore, the Sr-isotope ratios of the clinopyroxenes are higher than the whole rock (Table 2, Fig. 6), indicating that this phenocryst is largely derived from group 3 type magma. These findings are also in line with a lack of equilibrium in Mg–Fe partitioning between phenocrysts and bulk lavas (Jezek and Hutchison, 1978).

An important observation to be noted is the remarkable relation between oxygen isotopes and some incompatible trace-element ratios. Inverse correlations exist between $\delta^{18}O_{melt}$ and Zr/Nb (Fig. 10) and Th/Nb (not shown) ratios. The Serua trend deviates from curves that describe source mixing between depleted MORB mantle and bulk SCM or SCM-derived melt. The Zr/Nb-$\delta^{18}O_{melt}$ plot suggests that involvement of lower continental crust may be a more plausible alternative. Assimilation of lower crust with a Zr/Nb = 13 (Rudnick and Fountain, 1995) and $\delta^{18}O = 10$ by a typical Banda Arc magma is consistent with isotopic and trace-element signatures of the Serua lavas. Figure 14 shows that assimilation of average carbonate free sediment (CFS) is unlikely with reasonable parameters in an AFC model (DePaolo, 1981), and that sediments with low $\delta^{18}O$ appear to be a more appropriate end-member. The adopted end-member is represented by a sedi-

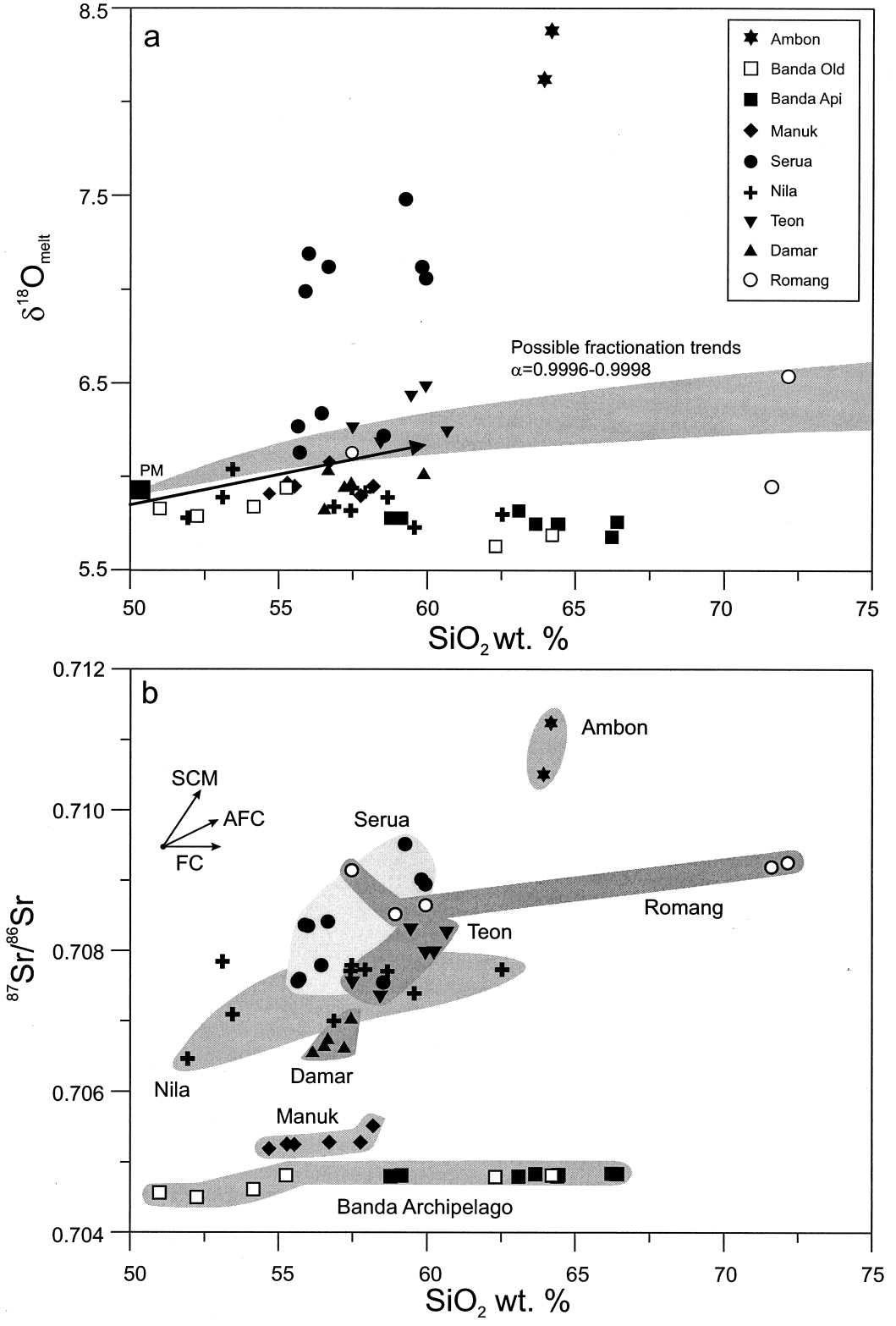

Fig. 13. SiO_2 versus (a) $\delta^{18}O_{melt}$ and (b) $^{87}Sr/^{86}Sr$ for Banda Arc volcanics. The shaded area in (a) indicates a calculated SiO_2 $\delta^{18}O_{melt}$ fractionation trend for a Banda Archipelago basalt with SiO_2 = 50%, $\delta^{18}O_{melt}$ = 5.7‰ and solid-melt fractionation coefficients (α) between 0.9996–0.9998 (cf. Woodhead et al., 1987). Note that most samples plot below or within this fractionation trend. The arrow indicates a trend observed in the 1982–1983 eruption products of Galunggung (Harmon and Gerbe, 1992). Abbreviations in (b): FC = fractional crystallization, AFC = assimilation fractional crystallization and SCM = subducted continental material. One anomalous sample from Nila plots outside the main trend and represents a mafic inclusion.

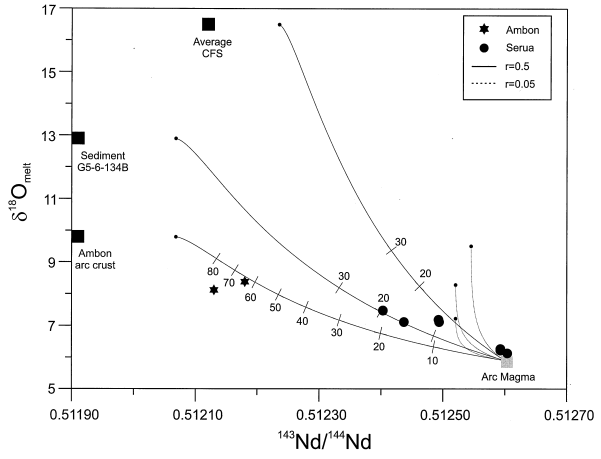

Fig. 14. AFC models (DePaolo, 1981) for Ambon and Serua volcanics. Tic marks indicate ρ (mass of crust assimilated/mass of original magma) as defined by Aitcheson and Forrest (1994). Curves for r = 0.5 and 0.05 are shown for three crustal end members: average carbonate free sediment (CFS), sediment 134B (see Table 3) and an estimate of Ambon crust. End-member compositions are given in Table 4. Bulk distribution coefficient: D_{Nd} = 0.2. See text for discussion.

ment sample (134B) from Track III (Fig. 1) which actually contains metamorphic pebbles (Vroon et al., 1995).

It is noteworthy that lavas from Ambon that bear evidence of extensive crustal assimilation (see below) plot close to the trend defined by Serua and the lower crust (Fig. 10). Furthermore, the presence of pieces of continental crust below Serua is conceivable, as (thinned) slivers of continental crust are common in the Banda Sea area, which is in agreement with a proposed back-arc spreading origin (Hamilton, 1979; Honthaas et al., 1998). Additional evidence for crustal assimilation has been derived from dredged lavas from the submarine Banda ridges (Morris et al., 1984; Honthaas et al., 1998). Both bulk assimilation and AFC models indicate approximately 10–20% assimilation for Serua (Figs. 9 and 14).

5.3.2. Nila

The presence of metasedimentary inclusions (Vroon et al., 1993) and a positive correlation between SiO_2 and $^{87}Sr/^{86}Sr$ [Fig. 13(b)] provide unequivocal evidence for assimilation in the lava suite of Nila island. Furthermore, Sr–Nd isotope relations can be interpreted in terms of bulk assimilation of local sediment (Vroon et al., 1993). However, in contrast to Serua, there is no positive correlation between SiO_2 and $\delta^{18}O_{melt}$. The discrepancy could be ascribed to a fortuitous similarity in the oxygen-isotopic signatures of assimilant and host, but a pre-assimilation origin of the clinopyroxene phenocrysts, from which we calculated the $\delta^{18}O_{melt}$, seems a more likely explanation. Petrographic and isotopic disequilibrium is a conspicuous feature in the Nila volcanics, given the presence of mafic magmatic inclusions having lower $^{87}Sr/^{86}Sr$ than their hosts (Vroon et al., 1993), and sedimentary carbonate–quartz inclusions with small reaction rims. Assimilation may thus have taken place in a short time span just before or during eruption, which corroborates the supposition that the analyzed phenocrysts record primary $\delta^{18}O$ signals.

5.3.3. Ambon

Unlike most other parts of the Banda Arc, the island of Ambon at its northern end where volcanic activity has ceased, is underlain by a metamorphic basement. High-K peraluminous andesites and dacites (ambonites; Van Bemmelen, 1949) are among the most common rock types. Abundant high-grade metasedimentary inclusions with Al-rich mineral assemblages probably represent schists and gneisses derived from a foliated basement similar to that exposed on the adjacent island of Seram (Van Bergen et al., 1989).

Several mechanisms have been proposed for the origin of the ambonites. Anatectic melting of metapelites was considered by Whitford and Jezek (1979) and Magaritz et al. (1978) who reported whole-rock $\delta^{18}O$ values of 14.1–16.7‰, whereas Linthout and Helmers (1994) invoked obduction-induced crustal anatexis due to Late Miocene ophiolite emplacement. However, the relatively high $\delta^{18}O_{melt}$ (8.1–8.4‰), compared to values from the active Banda Arc reported here, can be attributed to the effects of assimilation (Fig. 14). The melt data deduced from pyroxene phenocrysts are lower than whole-rock values of 14.1–16.7‰ obtained for ambonites (Magaritz et al., 1978), which commonly contain abundant xenolithic/crystic material. Furthermore, sample AM93A1 suggests isotopic disequilibrium between pyroxene and garnet, which has a higher $\delta^{18}O$ value of 9.76‰ and represents a relict of the metamorphic assemblage according to textural evidence.

These observations support the conclusion (Van Bemmelen, 1949; Honthaas, 1999) that subduction-related magmas were modified by large-scale assimilation of continental crust. The steep trend in the SiO_2–K_2O plot (Fig. 2) is consistent with the hypothesis that high-K magmas originated from low-K parental magma by this process. The parental basaltic (or intermediate?) magma may have been derived from a source that was contaminated by a subducted sedimentary component, in view of the relatively high $^{87}Sr/^{86}Sr$ (0.70423–0.70435; Whitford and Jezek, 1979) and low $^{143}Nd/^{144}Nd$ (~0.51275; Morris et al., 1984) of low-K pillow basalts in the southwestern part of Ambon, which represent the most mafic lavas on the island. The AFC modelling (Fig. 14) suggests large degrees of mobilization and assimilation (up to 80%) of crustal basement rocks with a moderately high $\delta^{18}O$ of ~10‰, consistent with the measured value of metamorphic garnet xenocrysts in lava sample AM93A1. The inferred large percentage of assimilated crustal material is supported by the abundance of metamorphic xenoliths and xenocrysts that characterize many of the ambonites (e.g., Van Bergen et al., 1989; Honthaas et al., 1999).

6. CONCLUSIONS

(1) Oxygen isotope data obtained from phenocrysts by the laser-fluorination method show that the Banda Arc magmas are characterized by mantle values ($\delta^{18}O_{melt}$ = 5.57–6.48‰), similar to those observed in other island arcs, with the exception of several lavas of Serua and Ambon for which higher ratios were found ($\delta^{18}O_{melt}$ < 8.4‰). The phenocryst data appear to record significantly lower $\delta^{18}O$ signatures for the Banda Arc magmas than can be deduced from conventional bulk-lava data, as in the pioneering study of Magaritz et al. (1978).
(2) The low $\delta^{18}O$ nature of the Banda Arc magmas can be

reconciled with the conclusions from Sr–Nd–Pb–Hf–He–Th–U isotopic studies (Vroon et al., 1995; Hoogewerff et al., 1997, and references therein), which point to contributions from subducted continental material (SCM) to magma sources that are the most extreme among the world's present-day active oceanic island arcs. According to these radiogenic isotope systems, up to 10% of SCM is involved, but mass-balance considerations, based on mixing between depleted Indian–MORB mantle and SCM melt, predict that $\delta^{18}O$ signatures of primary magmas will remain within the range of mantle values.

(3) Assimilation was important in the genesis of the high $\delta^{18}O_{melt}$ lavas of Serua and Ambon, where AFC modelling indicates that up to ~20% (Serua) or ~80% (Ambon) of (lower) continental crust may have contaminated primary arc magma. Conversely, petrographic and Sr–Nd isotopic evidence for assimilation in the lavas of Nila is not visible in oxygen isotope data, as $\delta^{18}O_{melt}$ values derived from clinopyroxene phenocrysts are not higher than the overall Banda Arc signatures. We hypothesize that this represents a case of rapid late-stage incorporation of arc–crust sediments without isotopic re-equilibration.

(4) Our findings suggest that, even in the case of a continent–arc collision, a large contribution of subducted sediments to magma sources may not be recorded in oxygen-isotope signatures of arc lavas. Hence, $\delta^{18}O$ values of $>6.5‰$ in arc magmas will commonly reflect shallow-level assimilation of crustal material.

Acknowledgments—This study forms part of a continuing research program in the Sunda-Banda Arc, carried out by the Volcanological Survey of Indonesia (VSI) and the Faculty of Earth Sciences of Utrecht University, in collaboration with the Southeast Asia Group of the University of London and the Faculty of Earth Sciences, Free University, Amsterdam. Dr. W. S. Tjetjep, Dr. R. Sukhyar, Dr. A. D. Wirakusumah and colleagues from VSI are kindly thanked for support during research and field work in Indonesia. We thank Alison MacDonald, Chris Taylor, and Kirsten Ross for expert technical assistance at the Scottish Universities Environmental Research Centre, Glasgow. Pier de Groot kindly provided whole-rock oxygen isotope data, using the stable-isotope laboratory at the Faculty of Earth Sciences, Utrecht University. Helpful discussions with Colin Macpherson, Jurian Hoogewerff, Matthew Thirlwall, Robert Hall, and Tim Elliott are gratefully acknowledged. The stable-isotope laboratory at Royal Holloway is an Intercollegiate Analytical Facility, part-funded by the University of London. We are grateful to John Eiler for a thorough and constructive review of the paper.

Associate editor: S. M. McLennan

REFERENCES

Abbott M. J. and Chamalaun F. H. (1981) Geochronology of some Banda arc volcanics. In *Geology and Tectonics of Eastern Indonesia* (ed. A. J. Barber) Indonesian Geological Research and Development Center Special Publication No. 2, pp. 253–268.

Ahmad S. M., Guichard F., Hardjawidjaksana K., Adisaputra M. K., and Labeyrie L. D. (1995) Late quarternary paleoceanography of the Banda Sea. *Marine Geology* **122,** 385–397.

Aitcheson S. J. and Forrest A. H. (1994) Quantification of crustal contamination in open magmatic systems. *J. Petrol.* **35,** 461–488.

Borthwick J. and Harmon R. S. (1982) A note regarding ClF_3 as an alternative to BrF_5 for oxygen isotope analysis. *Geochim. Cosmochim. Acta* **46,** 1665–1668.

Bowin C. O., Purdy G. M., Johnston C., Shor G. G., Lawver L., Hartono H. M. S., and Jezek P. (1980) Arc-continent collision in Banda Sea region. *Bull. Am. Assoc. Pet. Geol.* **64,** 868–915.

Clayton R. N. and Mayeda T. K. (1963) The use of bromine pentafluoride in the extraction of oxygen from oxides and silicates for isotope analysis. *Geochim. Cosmochim. Acta* **27,** 43–52.

Craig H. (1957) Isotopic standards for carbon and oxygen and correction factors for mass-spectrometric analysis of carbon dioxide. *Geochim. Cosmochim. Acta* **12,** 133–149.

Davidson J. P. (1985) Mechanisms of contamination in Lesser Antilles island arc magmas from radiogenic and oxygen isotope relationships. *Earth Planet. Sci. Lett.* **72,** 163–174.

Davidson J. P. (1987) Crustal contamination versus subduction zone enrichment: examples from the Lesser Antilles and implications for the mantle source composition of island arc volcanic rocks. *Geochim. Cosmochim. Acta* **51,** 2185–2198.

Davidson J. P. and Harmon R. S. (1989) Oxygen isotope constraints on the petrogenesis of volcanic arc magmas from Martinique, Lesser Antilles. *Earth Planet. Sci. Lett.* **95,** 255–270.

DeMets C., Gordon R. G., Argus D. F., and Stein S. (1994) Effect of recent revisions to the geomagnetic reversal timescale on estimates of current plate motions. *Geophys. Res. Lett.* **21,** 2191–2194.

DePaolo D. J. (1981) Trace element and isotopic effects on combined wall rock assimilation and fractional crystallization. *Earth Planet. Sci. Lett.* **53,** 189–202.

DeGroot P. A. (1993) Stable isotope (C, O, H) major- and trace element studies on hydrothermal alteration and related ore mineralization in the volcano-sedimentary belt of Bergslagen, Sweden. Ph.D. thesis, Utrecht University.

Edwards C., Menzies M., and Thirlwall M. (1991) Evidence from Muriah, Indonesia, for the interplay of supra-subduction zone and intraplate processes in the genesis of potassic alkaline magmas. *J. Petrol.* **32,** 555–592.

Edwards C. M. H., Menzies M. A., Thirlwall M. F., Morris J. D., Leeman, W. P., and Harmon R. S. (1994) The transition to potassic alkaline volcanism in island arcs; the Ringgit–Beser Complex, East Java, Indonesia. *J. Petrol.* **35,** 1557–1595.

Eiler J. M., Farley K. A., Valley J. W., Hofmann A. W., and Stolper E. M. (1996) Oxygen isotope constraints on the sources of Hawaiian volcanism. *Earth Planet. Sci. Lett.* **144,** 453–468.

Eiler J. M., Farley K. A., Valley J. W., Hauri E. H., Craig H., Hart S. R., and Stolper E. M. (1997) Oxygen isotope variations in ocean island basalt phenocrysts. *Geochim. Cosmochim. Acta* **61,** 2281–2293.

Eiler J. M., Crawford A., Elliott T., Farley K. A., Valley J. W., and Stolper E. M. (2000) Oxygen isotope geochemistry of oceanic-arc lavas. *J. Petrol.* **41,** 229–256.

Ellam R. M. and Hawkesworth C. J. (1988) Elemental and isotopic variations in subduction related basalts: evidence for a three component model. *Contrib. Mineral. Petrol.* **98,** 72–80.

Ellam R. M. and Harmon R. S. (1990) Oxygen isotope constraints on the crustal contribution to the subduction-related magmatism of the Aeolian Islands, southern Italy. *J. Volcanol. Geotherm. Res.* **44,** 105–122.

Elliott T., Plank T., Zindler A., White W., and Bourdon B. (1997) Element transport from slab to volcanic front at the Mariana Arc. *J. Geophys. Res.* **102,** 14991–15019.

Ferrara G., Laurenzi M. A., Taylor H. P., Tonarini S., and Turi B. (1985) Oxygen and strontium studies of K-rich volcanic rocks from the Alban Hills, Italy. *Earth Planet. Sci. Lett.* **75,** 13–28.

Ferrara G., Preite-Martinez M., Taylor H. P. Jr., Tonarrini S., and Turi B. (1986) Evidence for crustal assimilation, mixing of magmas and a ^{87}Sr-rich upper mantle: an oxygen and strontium isotope study of the M. Vulsini volcanic area, central Italy. *Contrib. Mineral. Petrol.* **92,** 269–280.

Gill J. B. (1981) *Orogenic Andesites and Plate Tectonics*. Springer-Verlag.

Gill J. B. and Williams W. R. (1990) Th isotope and U-series studies of subduction-related volcanic rocks, *Geochim. Cosmochim. Acta* **54,** 1427–1442.

Hamilton W. (1979) Tectonics of the Indonesian region. U.S. Geological Survey Professional Papers **1078,** pp. 1–345.

Harmon R. S. and Gerbe M. (1992) The 1982–1983 eruption at Gal-

unggung volcano, Java (Indonesia): oxygen isotope geochemistry of a chemically zoned magma chamber. *J. Petrol.* **33,** 585–609.

Harmon R. S. and Hoefs J. (1995) Oxygen isotope heterogeneity of the mantle deduced from global ^{18}O systematics of basalts from different geotectonic settings. *Contrib. Mineral. Petrol.* **120,** 95–114.

Hilton D. and Graig H. (1989) A helium isotope transect along the Indonesian archipelago. *Nature* **342,** 906–908.

Hilton D. R., Hoogewerff J. A., Van Bergen M. J., and Hammerschmidt K. (1992) Mapping magma sources in the east Sunda-Banda arcs, Indonesia: Constraints from helium isotopes. *Geochim. Cosmochim. Acta* **56,** 851–859.

Hoogewerff J. A., Van Bergen M. J., Vroon P. Z., Hertogen J., Wordel R., Sneyers A., Nasution A., Moens H. L. E., and Mouchel D. (1997) U-series, Sr–Nd–Pb isotope and trace element systematics across an active island arc continent collision zone: Implications for element transfer at the slab-wedge interface. *Geochim. Cosmochim. Acta* **61,** 1057–1072.

Honthaas C., Maury R. C., Priadi B., Bellon H., and Cotton J. (1999) The Plio-Quarternary Ambon Arc, Eastern Indonesia. *Tectonophysics* **301,** 261–281.

Honthaas C., Réhault J-P., Maury R. C., Bellon H., Hemond C., Malod J-A., Cornée J-J., Villeneuve M., Cotton J., Burhanuddin S., Guillou H., and Arnoud N. (1998) A Neogene back-arc origin for the Banda Sea basins: geochemical and geochronological constraints from the Banda Ridges (East Indonesia). *Tectonophysics* **298,** 297–317.

Ito E. and Stern R. J. (1985) Oxygen and strontium isotopic investigations of subduction zone volcanism: the case of the Volcano Arc and the Marianas Island Arc. *Earth Planet. Sci. Lett.* **76,** 312–320.

Ito E., White W. M., and Gospel C. (1987) The O, Sr, Nd and Pb isotope geochemistry of MORB. *Chem. Geol.* **62,** 157–176.

Jacobson R. S., Shor G. G., Kieckhefer R. M., and Purdy G. M. (1978) Seismic refraction and reflection studies in the Timor-Aru Trough system and Australian continental shelf. *Am. Ass. Petrol. Geol. Mem.* **29,** 209–222.

James D. E. (1981) The combined use of the oxygen and radiogenic isotopes as indicators of crustal contamination. *Ann. Rev. Earth. Planet. Sci.* **9,** 311–344.

Jezek P. A. and Hutchison C. S. (1978) Banda arc of eastern Indonesia: Petrography and geochemistry of the volcanic rocks. *Bull. Volc.* **41,** 586–608.

Johnson M. C. and Plank T. (1999) Dehydration and melting experiments constrain the fate of subducted sediments, *G3* **1,** Paper number 1999GC000014.

Kalamarides R. I. (1986) High-temperature oxygen isotope fractionation among the phases of Kiglapait intrusion, Labrador, Canada. *Chem. Geol.* **58,** 303–310.

Kelemen P. B., Johnson K. T. M., Kinzler R. J., and Irving A. J. (1990) High-field-strength element depletions in arc basalts due to mantle-magma interaction. *Nature* **345,** 521–524.

Kogiso T., Tatsumi Y., and Nakano S. (1997) Trace element transport during dehydration processes in the subducted oceanic crust: 1. Experiments and implications for the origin of ocean island basalts. *Earth Planet. Sci. Lett.* **148,** 193–205.

Lapouille A., Haryono H., Larue M., Pramumijoyo S., and Lardy M. (1985) Age and origin of the seafloor of the Banda Sea (eastern Indonesia). *Oceanol. Acta* **8,** 379–389.

Linthout K. and Helmers H. (1994) Plicene obducted, rotated and migrated ultramafic rocks and obduction-induced anatectic granite, SW Seram and Ambon, Eastern Indonesia. *J. Southeast Asian Earth Sci.* **9,** 95–109.

Macpherson C. G. (1994) New analytical approaches to the oxygen and carbon stable isotope geochemistry of some subduction-related lavas. Ph. D. thesis, University of London.

Macpherson C. G. and Mattey D. P. (1998) Oxygen isotope variations in Lau Basin lavas. *Chem. Geol.* **144,** 177–194.

Macpherson C. G., Gamble J. A., and Mattey D. P. (1998) Oxygen isotope geochemistry of lavas from an oceanic to continental arc transition, Kermadec-Hikurangi margin, SW Pacific. *Earth Planet. Sci. Lett.* **160,** 609–621.

Magaritz M., Whitford D. J., and James D. E. (1978) Oxygen isotopes and the origin of high-$^{87}Sr/^{86}Sr$ andesites. *Earth Planet. Sci. Lett.* **40,** 220–230.

Mattey D. P. and Macpherson C. G. (1993) High-precision oxygen isotope microanalysis of ferromagnesian minerals by laser fluorination. *Chem. Geol.* **105,** 305–318.

Mattey D. P., Lowry D., and Macpherson C. G. (1994) Oxygen isotope composition of the mantle. *Earth Planet. Sci. Lett.* **128,** 231–241.

McCrea J. M. (1950) On the isotope geochemistry of carbonates and a paleotemperature scale. *J. Chem. Phys.* **18,** 849–857.

McCulloch M. T., Compston W., Abbott M., Chivas A., Foster J. J., and Nelson D. R. (1982) Neodymium, strontium, lead and oxygen isotopic and trace element constraints on magma genesis in the Banda island-arc, Wetar. Research School of Earth Sciences Annual Report 1982, 236–238.

Morris J. D., Gill J. B., Schwartz D., and Silver E. A. (1984) Late Miocene to Recent Banda Sea volcanism, III: Isotopic compositions [abstract], *EOS Trans. AGU* **65,** 1135.

Pigram C. J. and Panggabean H. (1983) Age of the Banda Sea, eastern Indonesia. *Nature* **301,** 231–234.

Plank T. and Langmuir C. H. (1993) Tracing trace elements from sediment input to volcanic output at subduction zones. *Nature* **362,** 739–743.

Plank T. and Ludden J. (1992) Geochemistry of sediments in the Argo abyssal plain at site 765: A continental margin reference section for sediment recycling in subduction zones. In F. M. Gradstein, J. N. Ludden et al., Proc. ODP Sci. Results, Vol. **123,** 167–189.

Puntodewo S. S. O., McCaffrey R., Calais E., Bock Y., Rais J., Subarya C., Poewariardi R., Stevens C., Genrich J., Fauzi Zwick P., and Wdowinski S. (1994) GPS measurements of crustal deformation within the Pacific-Australia plate boundary zone in Irian Jaya, Indonesia. *Tectonophysics* **237,** 141–153.

Rudnick R. L. and Fountain D. M. (1995) Nature and composition of the continental crust; a lower crustal perspective. *Rev. Geophys.* **33,** 267–309.

Silver E. A., Gill J. B., Schwartz D., Prasetyo H., and Ducan R. A. (1985) Evidence for a submerged and displaced continental borderland, north Banda Sea, Indonesia. *Geology* **13,** 687–691.

Singer B. S., O'Neil J. R., and Brophy J. G. (1992) Oxygen isotope constraints on the petrogenesis of Aleutian arc magmas. *Geology* **20,** 367–370.

Smith T. E., Thirlwall M. F., and Macpherson C. (1996) Trace element and isotope geochemistry of the volcanic rocks of Bequia, Grenadine islands, Lesser Antilles arc: a study of subduction enrichment and intra-crustal contamination. *J. Petrol.* **37,** 117–143.

Staudigel H., Davies G. R., Hart S. R., Marchant K. M., and Smith B. M. (1995) Large scale isotopic Sr, Nd and O isotopic anatomy of altered oceanic crust: DSDP/ODP sites 417/418. *Earth Planet. Sci. Lett.* **130,** 169–185.

Stolz A. J., Varne R., Wheller G. E., Foden J. D., and Abbott M. J. (1988) The geochemistry and petrogenesis of K-rich alkaline volcanics from the Batu Tara volcano, eastern Sunda arc. *Contrib. Mineral. Petrol.* **98,** 374–389.

Stolz A. J., Varne R., Davies G. R., Wheller G. E., and Foden J. D. (1990) Magma source components in an arc-continent collision zone: the Flores-Lembata sector, Sunda Arc, Indonesia, *Contrib. Mineral. Petrol.* **105,** 585–601.

Taylor H. P., Jr., Turi B., and Cundari A. (1984) $^{18}O/^{16}O$ and chemical relationships in K-rich volcanic rocks from Australia, East Africa, Antartica and San Venanzo-Cupaello, Italy. *Earth Planet. Sci. Lett.* **69,** 263–275.

Thirlwall M. F., Graham A. M., Arculus R. J., Harmon R. S., and Macpherson C. G. (1996) Resolution of the effects of crustal assimilation, sediment subduction, and fluid transport in island arc magmas: Pb–Sr–Nd–O isotope geochemistry of Grenada, Lesser Antilles. *Geochim. Cosmochim. Acta* **60,** 4785–4810.

Tregoning P., Brunner F. K., Bock Y., Puntodewo S. S. O., McCaffrey R., Genrich J. F., Calais E., Rais J., and Subarya C. (1994) Estimation of current plate motions in Papua New Guinea from Global Positioning System. *J. Geophys. Res.* **103,** 12181–12203.

Valley J. W., Kitchen N., Kohn M. J., Niendorf C. R., and Spicuzza M. J. (1995) UWG-2, a garnet standard for oxygen isotope ratios: Strategies for high precision and accuracy with laser heating. *Geochim. Cosmochim. Acta* **59,** 5223–5231.

Van Bemmelen R. W. (1949) The geology of Indonesia, Volume 1A, Government Printing Office, The Hague.

Van Bergen M. J., Erfan R. D., Sriwana T., Suharyono K., Poorter

R. P. E., Varekamp J. C., Vroon P. Z., and Wirakusumah A. D. (1989) Spatial geochemical variations of arc volcanism around the Banda Sea. *Neth. J. Sea Res.* **24,** 313–322.

Van Bergen M. J., Vroon P. Z., Varekamp J. C., and Poorter R. P. E. (1992) The origin of the Potassic rock suite from Batu Tara volcano (East Sunda Arc, Indonesia). *Lithos* **28,** 261–282.

Van Bergen M. J., Vroon P. Z., and Hoogewerff, J. A. (1993) Geochemical and tectonic relationships in the East Indonesian arc-continent collision region: Implications for the subduction of the Australian passive margin. *Tectonophysics* **223,** 97–116.

Vroon P. Z. (1992) Subduction of continental material in the Banda Arc, Eastern Indonesia: Sr-Nd-Pb isotope and trace-element evidence from volcanics and sediments. Ph.D. thesis University of Utrecht.

Vroon P. Z., Van Bergen M. J., White W. M., and Varekamp J. C. (1993) Sr–Nd–Pb Isotope systematics of the Banda Arc, Indonesia: Combined subduction and assimilation of continental material. *J. Geophys. Res.* **98,** 22,349–22,366.

Vroon P. Z., Van Bergen M. J., Klaver G., and White W. M. (1995) Sr, Nd and Pb isotopic and trace-element signatures of the East Indonesian sediments: Provenance and implications for Banda Arc magma genesis. *Geochim. Cosmochim. Acta* **59,** 2573–2598.

Vroon P. Z., Van Bergen M. J., and Forde E. J. (1996) Pb and Nd isotope constraints on the provenance of tectonically dispersed continental fragments in East Indonesia. In *Tectonic Evolution of SE Asia* (eds. R. Hall and D. J. Blundell). *Geological Society Special Publication* **106,** 445–453.

Vroon P. Z., Nowell G., Hoogewerff J. A., and Van Bergen M. J. (1998) HFSE mobility at the slab-wedge interface: Hafnium-isotope evidence from the east Sunda-Banda arc. *Mineral. Mag.* **62A,** 1617–1618.

Whitford D. J., Compston W., Nicholls I. A., and Abbott M. J. (1977) Geochemistry of late Cenozoic lavas from eastern Indonesia: Role of subducted sediments in petrogenesis. *Geology* **5,** 571–575.

Whitford D. J. and Jezek P. (1979) Origin of the late Cenozoic lavas from the Banda arc, Indonesia: Trace element and Sr isotope evidence. *Contrib. Mineral. Petrol.* **68,** 141–150.

Whitford D. J., White W. M., and Jezek P. A. (1981) Neodymium isotopic composition of Quaternary island arc lavas from Indonesia. *Geochim. Cosmochim. Acta* **45,** 989–995.

Woodhead J. D., Harmon R. S., and Fraser D. G. (1987) O, S, Sr and Pb isotope variations in volcanic rocks from the northern Mariana Islands: implications for crustal recycling in intra-oceanic arcs. *Earth Planet. Sci. Lett.* **83,** 39–52.

Zheng Y.-F. (1993a) Calculation of oxygen isotope fractionation in anhydrous silicate minerals. *Geochim. Cosmochim. Acta* **57,** 1079–1091.

Zheng Y.-F. (1993b) Calculation of oxygen isotope fractionation hydroxyl-bearing silicates. *Earth Planet. Sci. Lett.* **120,** 247–263.